# Simultaneous parameter estimation and optimisation of a seeded anti-solvent crystallisation

Title: Simultaneous parameter estimation of a seeded anti-solvent crystallisation using a coupled Lasentec FBRM and ATR-FTIR method

Authors: Clifford T. Ó'Ciardhá[a*], Kieran W. Hutton[a] , Niall A. Mitchell[a], Patrick J. Frawley[b],
[a]Solids State Pharmaceuticals Cluster (SSPC), Materials and Surface Science Institute (MSSI), L1025, Lonsdale Building, Department of Mechanical, Aeronautical and Biomedical Engineering, University of Limerick, Castletroy, Co. Limerick, Ireland.
[b]Solids State Pharmaceuticals Cluster (SSPC), Materials and Surface Science Institute (MSSI), L1029, Lonsdale Building, Department of Mechanical, Aeronautical and Biomedical Engineering, University of Limerick, Castletroy, Co. Limerick, Ireland.

**Abstract**: A population balance incorporating nucleation, growth and agglomeration, solved using quadrature method of moments was coupled with a parameter estimation procedure. The seeded anti-solvent crystallisation of Paracetamol from methanol and water was chosen as the model system. All parameters concerned were regressed from moments calculated using the measured square weighted chord length distribution (CLD) generated by the FBRM. The FBRM and the concentration data are utilised together to obtain experimental moments that reflect the mass of solids in the tank. Using the estimated kinetic parameters, the crystallization model was validated using an additional experiment with a new non linear addition rate. Experimental crystal size distributions measured by laser diffraction are compared to CSDs calculated by the model and found to be in good agreement. No such work exists in the literature using FBRM to model an anti-solvent system which considers agglomeration. Based on the kinetic parameters estimated using the above method, the solution to the optimal anti-solvent addition rate profiles was obtained by applying nonlinear constrained multi-objective free final time formulation optimization on the validated model. These profiles were experimentally tested and CSD were compared with experiments used in the parameter estimation procedure. A 73.3% reduction in batch time was achieved with little impact on the CSD. Analyses of the various conflictions are presented with the aid of a pareto optimal plot to provide the practitioner with increased flexibility.

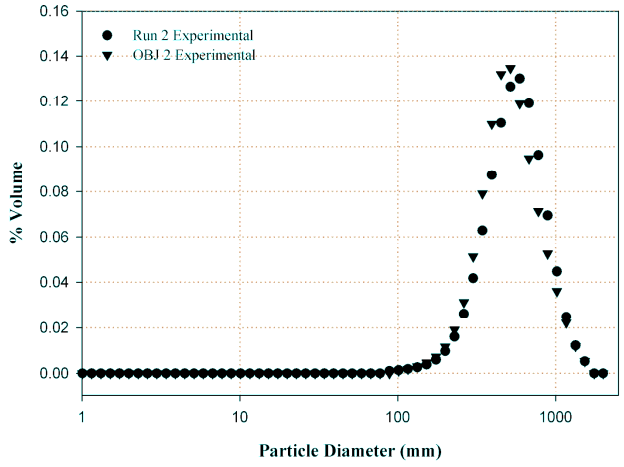


**Figure 13:** Experimental CSDs for objective 2 versus Run 2.

Clifford. T. Ó'Ciardhá
L1025, Lonsdale Building, Department of Mechanical, Aeronautical and Biomedical Engineering, University of Limerick, Castletroy, Co. Limerick, Ireland.
Tel: 00 353 61 213134
Fax: 00 353 61 202944
Email: clifford.ociardha@ul.ie

***Title Page***

Title: Simultaneous parameter estimation of a seeded anti-solvent crystallisation using a coupled Lasentec FBRM and ATR-FTIR method

Authors:

Clifford T. Ó'Ciardhá[a*]. Kieran W. Hutton[a] , Niall A. Mitchell[a], Patrick J. Frawley[b],

Affiliation:
[a]Solids State Pharmaceuticals Cluster (SSPC),
Materials and Surface Science Institute (MSSI),
L1025, Lonsdale Building,
Department of Mechanical, Aeronautical and Biomedical Engineering,
University of Limerick,
Castletroy,
Co. Limerick,
Ireland.

Email: clifford.ociardha@ul.ie
Email: niall.mitchell@ul.ie
Email: kieran.hutton@ul.ie

[b]Solids State Pharmaceuticals Cluster (SSPC),
Materials and Surface Science Institute (MSSI),
L1029, Lonsdale Building,
Department of Mechanical, Aeronautical and Biomedical Engineering,
University of Limerick,
Castletroy,
Co. Limerick,
Ireland.

Email: patrick.frawley@ul.ie

Corresponding Author:

Clifford. T. Ó'Ciardhá

L1025, Lonsdale Building,
Department of Mechanical, Aeronautical and Biomedical Engineering,
University of Limerick,
Castletroy,
Co. Limerick,
Ireland.

Tel: 00 353 61 213134
Fax: 00 353 61 202944
Email: clifford.ociardha@ul.ie

# Simultaneous parameter estimation of a seeded anti-solvent crystallisation using a coupled Lasentec FBRM and ATR-FTIR method

*Clifford Ó'Ciardhá*[*]*, Kieran Hutton, Niall Mitchell and Patrick Frawley*

Solid State Pharmaceuticals Cluster (SSPC), Materials and Surface Science Institute (MSSI),
Department of Mechanical, Aeronautical and Biomedical Engineering,
University of Limerick, Ireland.

A population balance incorporating nucleation, growth and agglomeration, solved using quadrature method of moments was coupled with a parameter estimation procedure. The seeded anti-solvent crystallisation of Paracetamol from methanol and water was chosen as the model system. All parameters concerned were regressed from moments calculated using the measured square weighted chord length distribution (CLD) generated by the FBRM. The FBRM and the concentration data are utilised together to obtain experimental moments that reflect the mass of solids in the tank. Using the estimated kinetic parameters, the crystallization model was validated using an additional experiment with a new non linear addition rate. Experimental crystal size distributions measured by laser diffraction are compared to CSDs calculated by the model and found to be in good agreement. No such work exists in the literature using FBRM to model an anti-solvent system which considers agglomeration. Based on the kinetic parameters estimated using the above method, the solution to the optimal anti-solvent addition rate profiles was obtained by applying nonlinear constrained multi-objective free final time formulation optimization on the validated model. These profiles were experimentally tested and CSD were compared with experiments used in the parameter estimation procedure. A 73.3% reduction in batch time was achieved with little impact on the CSD. Analyses of the various conflictions are presented with the aid of a pareto optimal plot to provide the practitioner with increased flexibility.

## 1. Introduction

Crystallisation is a widely used technique in solid–liquid separation processes and is regarded as one of the most important unit operations in the process industries as many finished chemical products are in the form of crystalline solids. The driving force in crystal formation is supersaturation. There are a number of methods to generate supersaturation such as cooling pH shift, evaporation of the solvent and anti-solvent addition. In anti-solvent crystallisation, supersaturation is generated by addition of another solvent or solvent mixture in order to reduce the solubility of the compound. Antisolvent crystallization is an advantageous method

where the substance to be crystallized is highly soluble, has solubility that is a weak function of temperature, is heat sensitive, or unstable at high temperatures[1]. Disadvantages of antisolvent crystallization include its high-dependency on mixing. Where poor mixing regimes exist, high local supersaturation at anti solvent addition zones exist leading to excess primary nucleation consequently resulting in fine crystal particle formation that easily tend to agglomerate[2]. Another disadvantage is that the anti-solvent can be difficult to recover and also the reduced operational capacity due to the addition of another solvent.

An optimized crystallization process is required to produce a desired crystal size distribution (CSD) as it strongly influences the quality of crystalline product and the efficiency of downstream operations. Achieving an optimal CSD can result in increased efficiency in product filterability solids handling. Hence, the control of the CSD involves designing an optimal model-based Addition rate profile to create the supersaturation profile required.[3-8]

The development of a model that can adequately describe the process and the ability to accurately estimate the parameters in the model is of significant importance since an optimisation can only be performed once the model is capable of predicting the CSD with a reasonable degree of confidence. Rigorous determination of an optimal batch recipe requires accurate estimation of growth and nucleation rate kinetics alongside empirical parameters for an agglomeration kernel if the system undergoes agglomeration, which can be determined in a series of batch experiments[9,10,11] Once the particle formation kinetics are known, they can be used together with a population balance model to simulate the influence of different process parameters on the final crystal size distribution (CSD) of the product. Omission of any of these attributes can lead to model-experimental discrepancies and a reduction in model optimisation efficacy.

One of the greatest challenges of estimating kinetic parameters is the accurate measurement of on line particle size and concentration. The evolution of on-line sensors such as FBRM and ATR-FTIR are offering new directions in solute concentration and particle size monitoring. The focused beam reflectance measurement technique offers unique advantages for a variety of industrial applications where in-situ monitoring of particle size or solid concentration is needed. There is a significant body of work in the literature which has utilized FBRM since its inception. It has been used for a variety of studies (experimental optimisation of crystallisation properties[12, 13, 14]). The properties of the FBRM itself have been extensively studied[15, 16]. These studies provide us with comprehensive reviews and comparisons of FBRM data with laser diffraction. Heath et al. found that the square-weighted

chord length was found to be comparable to laser diffraction, sieving, and electrical sensing zone analysis over the range of 50-400μm[15]. A similar result was reported by Yu et al. using PVC particles[16]. The FBRM gives a particle chord length distribution which is a function of the true particle diameter distribution. Conversion of the CLD into a CSD is not important for some applications because the relevant process variable can be correlated with some aspect of the chord length data. However the crystal size distribution (CSD) can be computed from the CLD, under certain assumptions using sophisticated mathematical algorithms[16-22].

To date there is very little work in the literature utilizing FBRM to supply particle size information for population balance modelling. Togkalidou et al. integrated the ATR-FTIR and FBRM to measure nucleation and growth kinetics for a cooling crystallisation[23]. Trifkovic et al uses a similar approach for the anti-solvent crystallisation of paracetamol[24]. Both works neglect agglomeration in their models and utilize moments regressed direct from the CLD. It will be shown in some detail in this paper that such an approach does not lead to accurate data for the purpose of population balance modelling.

This article describes a more rigorous approach to simultaneously estimate the nucleation and growth kinetics as well as empirical parameters for the chosen agglomeration kernel from anti-solvent batch experiments. This is achieved using a model of the crystallization process with dynamic population and mass balance equations. To date there has also been very little work done on modelling agglomeration in batch crystallisers[25, 26, 27].

Experimental data obtained from in situ measurements of the solution concentration using ATR-FTIR spectroscopy and in situ measurements of the square weighted Chord length distributions using laser backscattering are used to identify the parameters in the model. This approach is applied to the determination of the crystallization kinetics of paracetamol from methanol and water.

The identified model is used to optimise the crystal size distribution and batch time by applying nonlinear constrained multi-objective optimization on the validated model with final batch time, fines, particle mean size and the coefficient of variation as objectives to be optimized. The main focus of this paper was to reduce the process time as this would give the greatest financial saving, since most crystallisation processes are used for the production of intermediates which are re-dissolved for subsequent use. In this case an optimal CSD is one which can be produced in the shortest amount of time possible whilst not impeding downstream filtration processes. Additional targets such as fines, the coefficient of variation

and means particle size were included to inhibit the model deteriorating these characteristics during the optimisation process.

## 2. Experimental

### *2.1 Materials*

The experimental work outlined was performed on Acetaminophen A7085, Sigma Ultra, ≥99%, sourced from Sigma Aldrich. The methanol employed in this work was gradient grade hiPerSolv CHROMANORM for HPLC ≥99%, sourced from VWR.

### *2.2 Apparatus and experimental procedure*

The reactor is a baffled 1L round-bottomed borosilicate glass jacketed reactor, allowing controlled heating and cooling of solutions. All experiments are carried out isothermally at 25˚C. Agitation of the solution is provided by means of an overhead motor and a glass stirrer, with four blades at a pitch of $45^0$. The agitation is kept constant for all experiments at a value of 250 rpm. The system allows fluid dosing and the use of in-situ immersion probes. The system comes with iControl LabMax™ Software enabling real-time measurement of vital process parameters. Anti-solvent (water) addition into the solution was achieved using a ProMinent beta/4 peristaltic pump. An electronic balance (Mettler Toledo XS60025 Excellence) was used for recording the mass of anti-solvent added to the solution. Particle size distribution of the seed and final product was measured by a Horiba L92O Particle Size Analyser.

A Mettler-Toledo Focused Beam Reflectance Measurement (FBRM®) D600L probe was utilised in this work to track the evolution of the CLD during all experiments. For all FBRM® measurements, the fine detection setting was employed. The instrument provides a chord length distribution evolution over time at 30 second intervals.

A typical experimental procedure consisted of the following: The crystallizer was charged with a given amount of paracetamol (acetaminophen) and a solvent mixture of methanol and water. The batch temperature was raised to 30 °C and kept constant until all crystals were confirmed to be dissolved by FBRM. The temperature was then lowered to 25 °C to start the experiment. The experiments for the purpose of parameter estimation consisted

of four seeded experiments with constant addition rates ranging between 1-4 g/min and a subsequent validation experiment under an alternative variable addition rate shown in figure 10. The initial concentration was equal to or slightly greater than the solubility point at 25°C. The anti-solvent free solubility curve (expressed on a per kg of methanol basis), is shown elsewhere[28]. The seed loading employed was 3% of the theoretical yield for all experiments. This was chosen on the basis of experimental observations where a 3% seed loading gave sufficient information for the estimation of nucleation kinetic parameters whilst limiting excessive primary nucleation to avoid fouling of the probe. The initial mass of the solution in all of the experiments was 300 g, and an additional 250 g of water was added. All experimental conditions are reported in table 1.

**Table 1**: Experimental conditions and constraints.

| Variable | Name | Value | Units |
|---|---|---|---|
| $k_v$ | Shape factor | 0.866 | - |
| $L_0$ | Critical nucleus size | 1 | μm |
| $\rho_c$ | Crystal density | 1332 (ref 32) | kg/m$^3$ |
| $M_{MeOH+H20}$ | Initial mass of solvent | 0.3 | kg |
| $C_0$ | Initial concentration | 0.37 | kg/kg methanol |
| $C^*$ | Saturation concentration | See ref 36 | kg/kg methanol |
| $T$ | Temperature | 25 | ˚C |
| $M_w$ *initial* | Initial water mass fraction | 0.4 | - |
| $M_w$ *final* | Final water mass fraction | 0.67 | - |
| $R_{min}$ | Minimum Addition rate bound | 0.5 | g/min |
| $R_{max}$ | Maximum Addition rate bound | 10 | g/min |
| $M_{seed,\ min}$ | Minimum seed load | 0.2 | % |
| $M_{seed,\ max}$ | Maximum seed load | 9 | % |
| $R$ | Agitation | 250 | RPM |

## 3. Model Formulation

In a perfectly mixed batch reactor the evolution of the crystal size distribution can be described as follows:

$$\frac{\partial n(L,t)}{\partial t} + G(t)\frac{\partial n(L,t)}{\partial L} + J\delta(L - L_0) = B - D \quad (1)$$

where *n(L,t)* is the population density of the crystals and *G(t)* is the crystal growth rate which is assumed to be independent of size. The growth rate of crystals was assumed to be independent of size. Such assumptions are common in the industrial crystallization literature[29].

As the total working volume of the fed-batch crystalliser is constant, the population density and other relevant quantities will be defined on the basis of the solvent mass present. The population density function is stated in units of particle number per unit length per unit solvent (methanol) mass. Hence the model is formulated on an anti-solvent free basis. This model has been previously used to determine growth kinetics independently[28]. The agglomeration mechanism is represented by empirical birth *B* and death functions *D*, respectively. The agglomeration equation can be expressed in terms of the number density function using particle length as the internal coordinate. The agglomeration of two particles of length $\lambda$ and $L$–$\lambda$ into a new particle of length $\lambda$ is mathematically formulated by the rate of particle appearance:

$$B(L) = \frac{L^2}{2}\int_0^L \frac{\beta((L^3-\lambda^3)^{\frac{1}{3}},\lambda)}{(L^3-\lambda^3)^{\frac{2}{3}}} \times n\left((L^3-\lambda^3)^{\frac{1}{3}}\right) n(\lambda) d\lambda \quad (2)$$

And the rate of particle disappearance of length *v*:

$$D(L) = n(L)\int_0^\infty \beta n(L,\lambda) n(\lambda)\, d\lambda \quad (3)$$

The agglomeration kernel defined as

$$\beta = a_1 G^{a_2} \varepsilon^{a_3} \quad (4)$$

where

$$\varepsilon = \frac{N_p d_{imp}^5 n_s^3}{V} \quad (5)$$

where $N_p$ is the power number for the stirrer, $d_{imp}$ is the impeller diameter, $n_s$ is the stirring rate, and $V$ is the reactor volume. The evaluation of parameters $a_1$, $a_2$, $a_3$, will be discussed in

section 3.2. For a four blade impeller, a Power number of 1.08 has been estimated previously by Chapple et al.[30].This is a measure of the frequency of collisions between particles of length $\lambda$ and $L-\lambda$ that are successful in producing a particle of length $\lambda$. It is assumed to be independent of the crystal size. This empirical kernel was reported for modelling the agglomeration of L-Glutamic acid crystals[31]. The choice of kernel was governed by experimental observations. An increased level of agglomeration was observed with increasing growth rates. It will be shown in later sections that satisfactory results were achieved with the selection of the above agglomeration kernel expression. Size dependent expressions were tested and found to yield only minor improvements to the overall model to experimental data fit; however the size dependent kernel achieved this minor improvement at the expense of the higher order moments such as the third and fourth moment. With this in mind it was decided to pursue with the simpler size independent kernel. The evaluation of parameters in eq 4 will be discussed in more detail in section 3.2. The $k^{th}$ moment of the crystal size distribution can be described as:

$$\mu_k = \int_0^\infty n(L,t)L^k dL \tag{6}$$

During the crystallisation process, the mass balance of the solution phase can be described as:

$$\frac{dc}{dt} = -3k_v\rho_c G \int_0^\infty n(L,t)^2 dL \tag{7}$$

where $\rho_c$ and $k_v$ are the solid density and the volume shape factor of paracetamol crystals, respectively. The shape factor remains constant throughout the simulation duration. A value of 1332 kg/m$^3$ will be employed for the crystal density of form I of paracetamol[32]. The solution of eqs 6 and 7 requires an appropriate boundary and initial conditions, which are given as,

$$C(0) = C_0 \tag{8}$$

$$n(L,0) = n_{seed}(L)$$

with $C_0$ being the initial concentration of the solute, $n_{seed}(L)|t_0$ is the population density of seeds at time zero. The initial moments of the seed crystals are calculated from laser diffraction analysis. The particle size distribution of the seed crystals, prepared on an earlier date were measured. The moments of this distribution are calculated according to eq 6. The moments are then normalised with the third moment and converted into a per methanol basis as per eq 15. Typically, you cannot infer the zeroth moment from laser diffraction as this only gives a probability density function. However coupling the moments with the mass of crystals inferred from on line concentration data and the knowledge of the crystal density gives the number of crystals or zeroth moment of the seed crystals. This method is explained in more detail in section 3.2. The same procedure is applied to the moments calculated from the CLDs. The critical nucleus size in this work is given as 1μm as this is the minimum bin size of the FBRM probe used in this work to measure newly nucleated crystals. The supersaturation correlation used in this work is absolute supersaturation given as:

$$\Delta C = C - C^* \tag{9}$$

where $C$ is solute concentration and $C^*$ is the anti-solvent free solubility. The anti-solvent free solubility is calculated and described by Ó'Ciardhá et al.[28]. The size independent growth equation can be defined as:

$$G = k_g(\Delta C)^g \tag{10}$$

where $k_g$ is the growth rate constant. The exponent *g* denotes the growth order. The secondary nucleation expression is defined as.

$$J = k_n(\Delta C)^n(\mu_2)^{n_{sec}} \tag{11}$$

where, $k_n$ is nucleation rate constant, the exponent $n$ is the nucleation order and the exponent on the second moment $n_{sec}$ is the secondary nucleation order. Both growth and nucleation expressions are of an empirical nature. The evaluation of these parameters will be discussed in more detail in section 3.2. The crystal size distribution was reconstructed from the moments utilising a novel technique developed by Hutton et al[33].

### *3.1 Solution of the population balance equation*

Traditionally the population balance equation can be solved by either the widely published classes method, method of characteristics or method of moments, however the above equation cannot be solved by the standard method of moments due to the closure problem, therefore the quadrature method of moments (QMOM) is needed. The quadrature method of moment (QMOM) is based on the following transformation.

$$\mu_k(t) = \int_0^\infty nL^k dL = \sum_{j=1}^N \omega_j L_j^k \tag{12}$$

After moment transformation and applying the quadrature rule the agglomeration model is given by:

$$\frac{d\mu_k}{dt} = \frac{1}{2}\sum_{i=1}^N \omega_i \sum_{j=1}^N \omega_j \left(L_i^3 + L_j^3\right)^{\frac{k}{3}} \beta\left(L_i, L_j\right) - \sum_{i=1}^N \omega_i L_i^k \sum_{j=1}^N \omega_j \beta\left(L_i, L_j\right) + \sum_{i=1}^N \omega_i k L_i^{k-1} G + L_0^k J \tag{13}$$

Where, $L$ are the abscissas and $w$ are the quadrature weights. $L_0$ is the critical nucleus which is set at the minimum detectable size of the FBRM. Previous work by Marchisio et al has shown that a quadrature approximation with three nodes ($N=3$) was found to be a good trade off between accuracy and computational cost[34], therefore a three node quadrature approximation has been chosen for this work. The weights and abscissas are obtained with a recursive orthogonal polynomial generation algorithm according to Hutton (2009)[35].

### *3.2 Parameter estimation.*

In crystallisation the nucleation and growth of the solute molecule is governed by the driving force or supersaturation. Both of these phenomena compete for all available supersaturation. By altering the degree of supersaturation in the system one can weight the system to a higher degree of growth and/or nucleation. Therefore in a parameter estimation procedure, varying the supersaturation by means of varying the addition rate allows all the conditions that may occur in a crystallisation system to be captured by a single set of model parameters.

The data gathered for this purpose were from experiments undertaken in a seeded 1-L laboratory scale batch crystallizer under various anti-solvent addition profiles described in section 2.2.
To estimate these kinetic parameters ($k_g$, $g$, $k_n$, $n$, $n_{sec}$, $a_1$, $a_2$, $a_3$), the model is fitted to the experimental data by a nonlinear least-squares technique. The experimental data used includes the measurements from the ATR-FTIR and focused beam reflectance measurement (FBRM). Concentration was inferred from ATR-FTIR data using a previously reported method described by Ó'Ciardhá et al.[28].

In this study, the square weighted chord length distributions measured by FBRM were used to estimate the moments of the particle population density using eq 14 below, without converting the CLD measurements to a CSD. The CLD information from 1 to 1000μm was collected in 100 channels. The interval time was 30 seconds.

$$\mu_{k,FBRM} = \sum_{i=1}^{1000} L_i^k \, N_i(L_i t) \tag{14}$$

where $L_i$ and $N_i$ are the chord length and the square weighted count in the *ith* channel and t is the discrete time counter. Further treatment involves relating the moments to the mass of solids in the vessel by means of eq 15. Normalisation of all moments with respect to the third moment achieves moments per $m^3$ of solids. This is further converted to moments per kg of methanol. This results in moments that are reflective of the mass in the tank with the mass $m_c$ provided by the experimental concentration data.

$$\mu_{k,FBRM} = \left( \frac{\frac{\mu_k}{\mu_3}}{\rho_c k_v} \right) \frac{m_c}{m_s} \tag{15}$$

As a result of this operation the method then inherently utilizes both sets of data simultaneously. All moments are reflective of the mass of solids in the tank as a function of time leading to increased accuracy. For increased accuracy the number based moments of the seed distribution $\mu_{k(seed)}$ are calculated and added to the time derivative of the CLD moments estimated from eq 15. A CLD distribution is not reflective of a true particle size distribution hence we cannot use the data directly. Since the dynamic mapping of the CLD to a CSD should be the same, calculating the derivative of the experimental FBRM moments and initializing with moments calculated from PSDs measured by laser diffraction as can be

seen from eq 16 below, we avoid any drawbacks associated with un-weighted FBRM CLD data. These drawbacks include under sizing the particle diameter and overestimating the number of crystals present in the system. Another drawback to consider when using un-weighted CLDs is that at high solids loadings the CLDs taper off and will not increase with increasing solids loadings. Instead the derivative of the square weighted FBRM CLDs coupled with actual seed particle size data and the crystal mass is used as can be seen in eq 16.

$$\mu_k = \mu_{k(seed)} + \frac{d\mu_{k,FBRM}}{dt}\Delta t \tag{16}$$

Calculating moments directly from un-weighted CLDs underestimated the particle size and overestimated the number of particles. As a result it is not possible to use the un-weighted CLDs in modelling this process for reasons mentioned above. As expected these gave unrealistic parameters when the parameter estimation procedure was applied. It was found that when comparing the gradients of number based moments measured by laser diffraction that the square weighted distributions were the most comparable. When eq 16 is used, the higher order moments of the square weighted moments were more agreeable than those of the un-weighted moments. This process is not only justified by the necessity to avoid the aforementioned problems with un-weighted CLDs but the parameters obtained are reasonable, have good confidence intervals and are comparable with the literature

In an anti-solvent crystallization, the solvent mass is a dynamic quantity, however in this work the process is treated as a constant volume simulation. This is made possible by conversion of solubility data from g/g solution to g/g solvent, which simplifies the model and resembles that of a cooling crystallisation. This is known as anti-solvent free solubility. The entire crystallisation is modelled in the solvent and not the solution rendering any dilution term unnecessary. This also allows for estimation of the Metastablezone width from FBRM moments and concentration data as conducted previously by Ó'Ciardhá et al[36]. It also enables visualisation of the effect of phenomena such as secondary nucleation or the effect of increased seed mass from figure 16. This has a significant advantage in visualising results achieved by a numerical optimisation.

For the estimation of the parameters, the following nonlinear least-squares problem had to be solved:

$$\min(\theta)\left\{R = \sum_{i=1}^{N_{ex}} \sum_{j=1}^{N_m} \sum_{k=1}^{Nd} w_{ijk}\left[y_{ijk}^{meas} - y_{ijk}^{sim}(\theta)\right]^2\right\}$$

(17)

where $\theta$ is the set of parameters to be estimated, $y_{ijk}^{sim}$ represents the predicted model outputs in the k$^{th}$ intervals, $y_{ijk}^{meas}$ represents the variables measured with FBRM and ATR-FTIR at k$^{th}$ interval also. $N_d$ is the number of sampling instances, $N_{ex}$ is the number of experiments, $N_m$ is the number of measured variables where $m = [\mu_0, \mu_1, \mu_2, \mu_3, \mu_4, \mu_5, C]$ and $\theta = \left[k_g, g, k_n, n, n_{sec}, a_1, a_2, a_3\right]$. An altered, bounded version of the MATLAB optimisation algorithm *fminsearchbnd* which employs a Nelder-Mead simplex method was utilised to find the optimal set of parameters. The objective function (Eq. 17), consisting of a simple sum of squared errors, is often unsatisfactory because of several reasons, such as different scales of measurement or various physical dimensions. Also, some observations may be known to be less reliable than others, and parameter estimates should be less influenced by those than by more accurate ones. In this instance the third moment is most accurate as all moments are scaled with the third moment. Since solute concentration is analogues with the third moment a significantly higher weight is given to this data set. The solution to this problem is given by the method of weighted least squares. Since the error structure of eq 17 is unknown, eq 18 is chosen to provide a nonnegative weight.

$$w = \left(\frac{1}{\max\left(\left(y_{ijk}^{meas}\right)^2\right)}\right) \tag{18}$$

In this work a higher weight is given to the solute concentration data as the method depends on a high quality fit of this data due to the operation of eq 15. As a direct consequence of this, a higher weighting the third moment (u3) will be achieved.

To evaluate the robustness of the identified model, the confidence intervals of the estimated parameters were calculated. The confidence intervals were calculated using the t test as per eq 19[37].

$$\theta = \theta^* \pm t_{\frac{\alpha}{2}, N_{\mathrm{df}}} \sqrt{\mathrm{diag(V)}} \tag{19}$$

where $\theta^*$ is the estimated parameter vector and $t_{\frac{\alpha}{2},N_{\mathrm{df}}}$ is the t distribution with $N_{\mathrm{df}}$ degrees of freedom. The 95% confidence intervals are obtained for α=0.05. This procedure requires the estimation of the covariance matrix V.

$$V = S_R^2 P \tag{20}$$

where $S_R^2$ is the error variance described by $S_R^2 = R/N_{df}$ with $N_{df} = N_m(N_{ex}+1) - N_\theta - 1$ as the degrees of freedom. The Precision matrix P is given by

$$P = \left(J_\theta^T J_\theta\right)^{-1} \tag{21}$$

The Jacobian matrix *J* is a partial derivative matrix of model outputs *m* with respect to parameter vector $\theta$

$$J = \frac{\partial m}{\partial \theta} \tag{22}$$

## 4. Results and discussion

### 4.1 Parameter estimation

The estimated nucleation and growth kinetic parameters, as well as the empirical parameters for agglomeration found in eqs 4, 10 and 11 respectively are estimated based on four independent experiments. The estimation activities for all experiments were executed successfully and parameter values obtained are displayed in Table 2 along with their respective confidence intervals. This was possible from data collected from four experiments under constant addition rates. These experiments provide a range of supersaturations so that the model will have the capability of predicting quantities over a wide range of supersaturation values. In this case, any addition rate higher than 4g/min is not advisable as the measurement noise increases and provides inaccurate data. An additional experiment with an alternative addition rate to that used in the parameter estimation experiments was carried out for the purpose of validating the estimated parameters. The accuracy of the global parameters will be discussed by comparing experimental product CSDs with CSDs computed by the model. Predictions of the FBRM moments and ATR-FTIR concentration will also be

shown for each experiment. The models ability to reproduce the final CSD will be discussed and the validated experiment will be used alongside the confidence intervals to discuss the models efficacy in predicting the crystallisation system.

The low-order moments calculated from FBRM CLDs used in the parameter estimation procedure along with solute concentration data are shown in figures 1 to 4 along with the corresponding simulated data for Runs 1 to 4. For all experiments close agreement can be seen for the predicted and measured solute concentration and the low-order moments. Some discrepancies can be seen between the simulated and experimental zeroth moment. Overall, the prediction of the moments can be considered quiet satisfactory. This is more evident in run 4 (figure 4) as this is the highest addition rate employed in this work. Higher addition rates create more instrument noise and hence increased error and measurement uncertainties. In relation to data obtained from FBRM, an increased addition rate generates an increased production of entrained bubbles as the anti-solvent is added above the surface to avoid fouling. Bubbles are measured as particles in solution and add to the statistics of the instrument thereby increasing the total number of counts measured by the instrument. As can be seen from figures 1 to 4 a decreasing addition rate produces an increased quality of fit to the experimental data. Run 1 (Figure 1) corresponds to an addition rate of 1g/min and displays a significantly increased capability of predicting the zeroth moment due to the reduced level of measurement noise. An additional factor may be the statistical treatment of the experimental data. Obtaining a more accurate prediction of the zeroth moment should not be expected for a variety of reasons. The moments utilized in this work are calculated from square weighted CLDs. Square weighted CLDs are likely to provide a higher weight to the larger particles present in the system. Square weighting is an essential step in preparing data for use in a parameter estimation procedure as un-weighted CLDs over estimate crystal numbers. When the FBRM measures an individual crystal it takes a chord length of the crystal and not the true crystal diameter. As a result of this the probability of the laser estimating the correct crystal size can be low and decreases with increasing particle size. The laser can take a smaller chord length of the crystal and this value will be inserted into particle bins of a lower diameter. This effect significantly increases the estimated number of smaller crystals and reports on average a significantly reduced average particle size. Square weighting a CLD reduces this effect although it may skew the zeroth moment. This skewness diminishes as the moment number (k) increases. It can be seen in all plots that the model fit improved with increasing moment number. Since the model is calculated with accurate concentration data and this data is coupled to the FBRM data the error of the moments

increase as they deviate from the third moment since the third moment is directly proportional to the solute concentration. Alternatively, the higher level of discrepancy in run 3 (4g/min) could be attributed to model inadequacies. It is possible that at such an addition rate there is a higher generation of primary nuclei which the model does not predict. However due to the measurement noise in the experiments at higher addition rates it is very difficult to validate if the discrepancy is due to model inadequacies.

**Table 2:** Values of the estimated parameters along with confidence intervals for each parameter.

| *Parameters* | *Estimate* ***(Confidence Interval 95%)*** |
|---|---|
| *Ln kg* | -12.47 ± 5.5 |
| *g* | 1.12 ± 0.02 |
| *Ln kn* | 19.81 ± 9.18 |
| *n* | 1.48 ± 0.03 |
| $n_{sec}$ | 0.25 ± 0.02 |
| $a_1$ | 0.27 ± 0.22 |
| $a_2$ | 1.34 ± 0.01 |
| $a_3$ | 2.24 ± 0.37 |

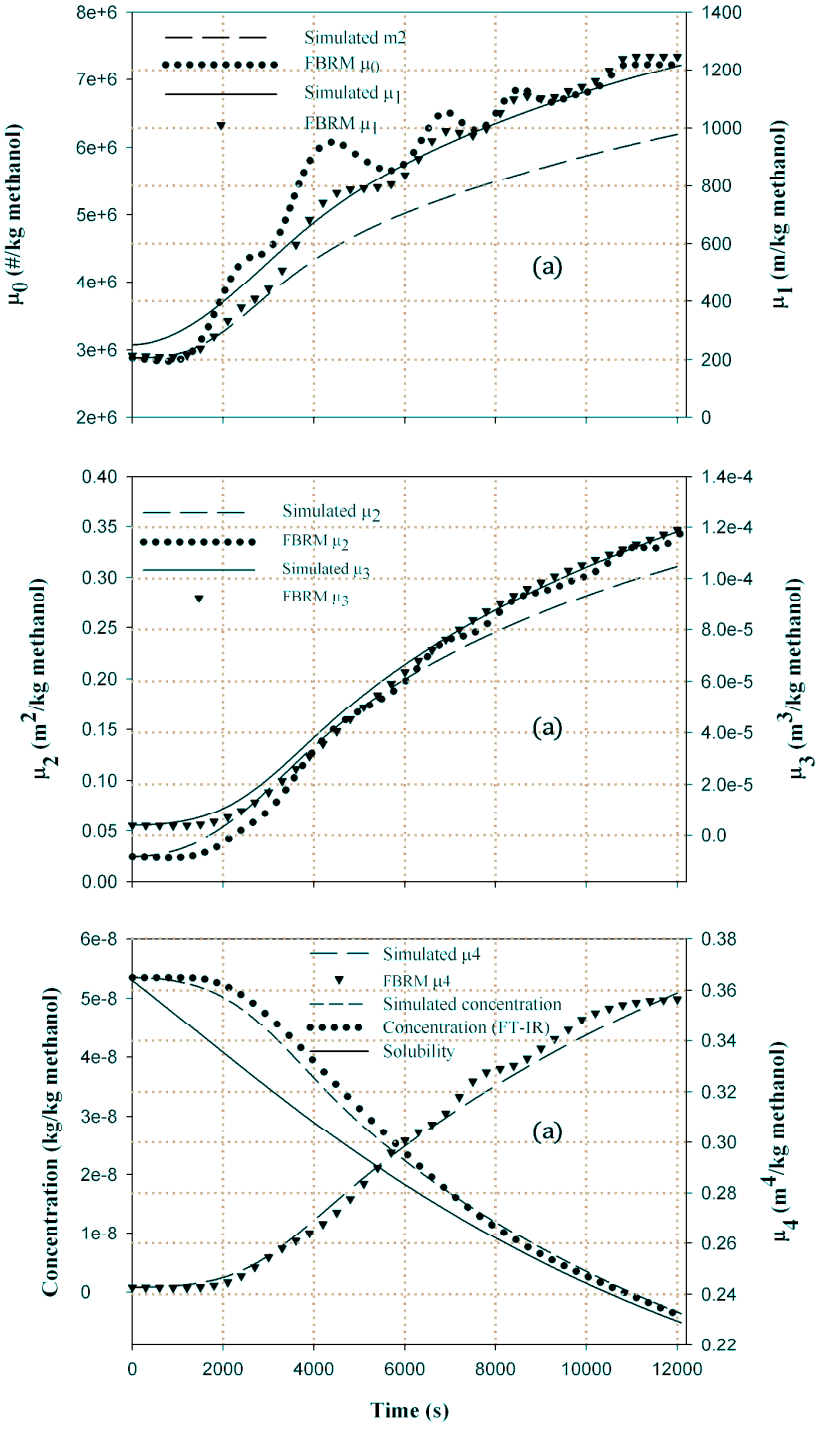


**Figure 1:** Results of Run 1 at a constant addition rate of 1g/min. Overlay plots of experimental FBRM CLD moments calculated using eq 16 and solute concentration against corresponding simulated data. (a) zeroth and first order FBRM moments (b) second and third order FBRM moments (c) fourth order FBRM moment, experimental solute concentration with corresponding simulated data.

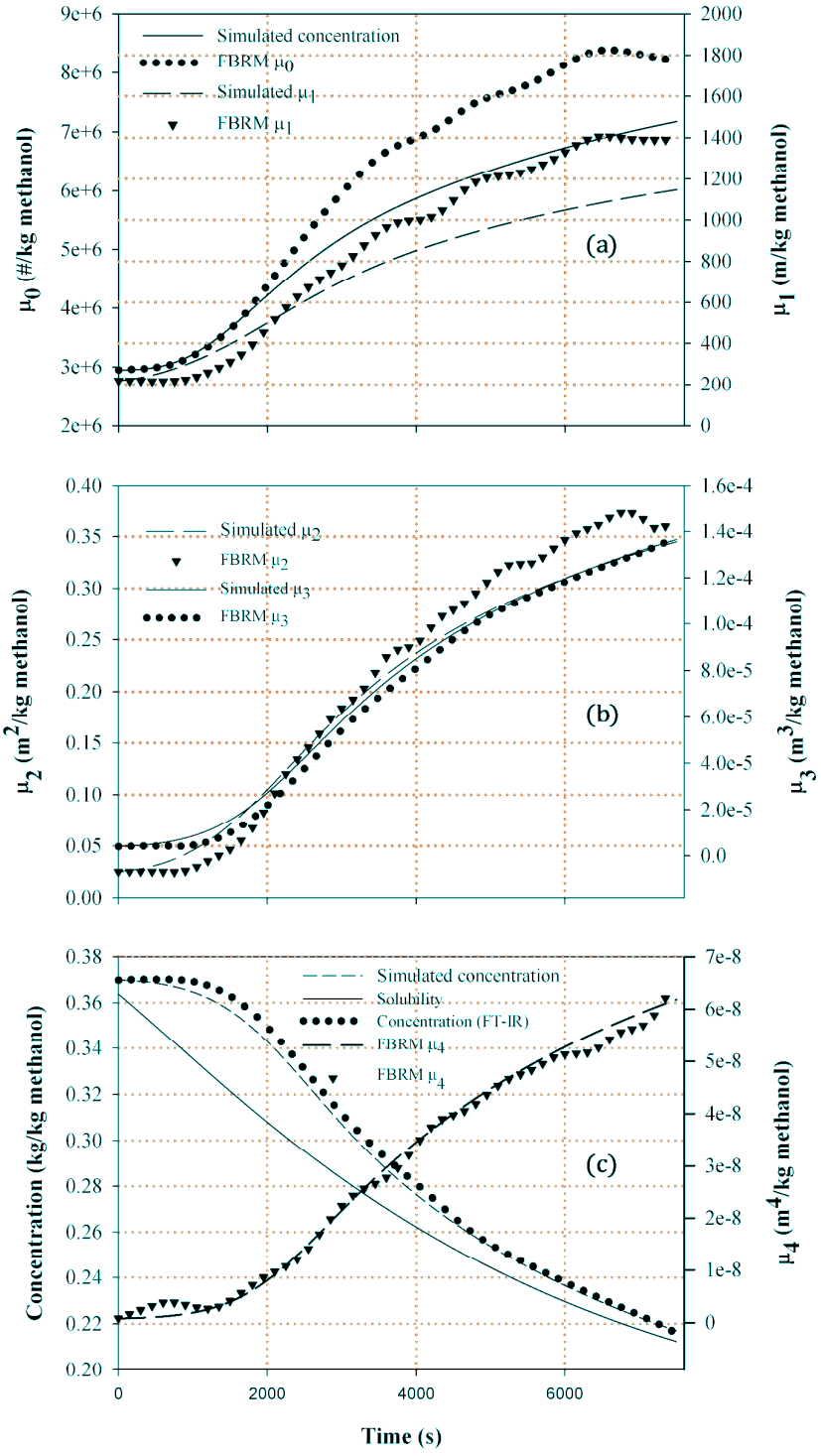


**Figure 2:** Results of Run 2 at a constant addition rate of 2g/min. Overlay plots of experimental FBRM CLD moments calculated using eq 16 and solute concentration against corresponding simulated data. (a) zeroth and first order FBRM moments (b) second and third order FBRM moments (c) fourth order FBRM moment, experimental solute concentration with corresponding simulated data.

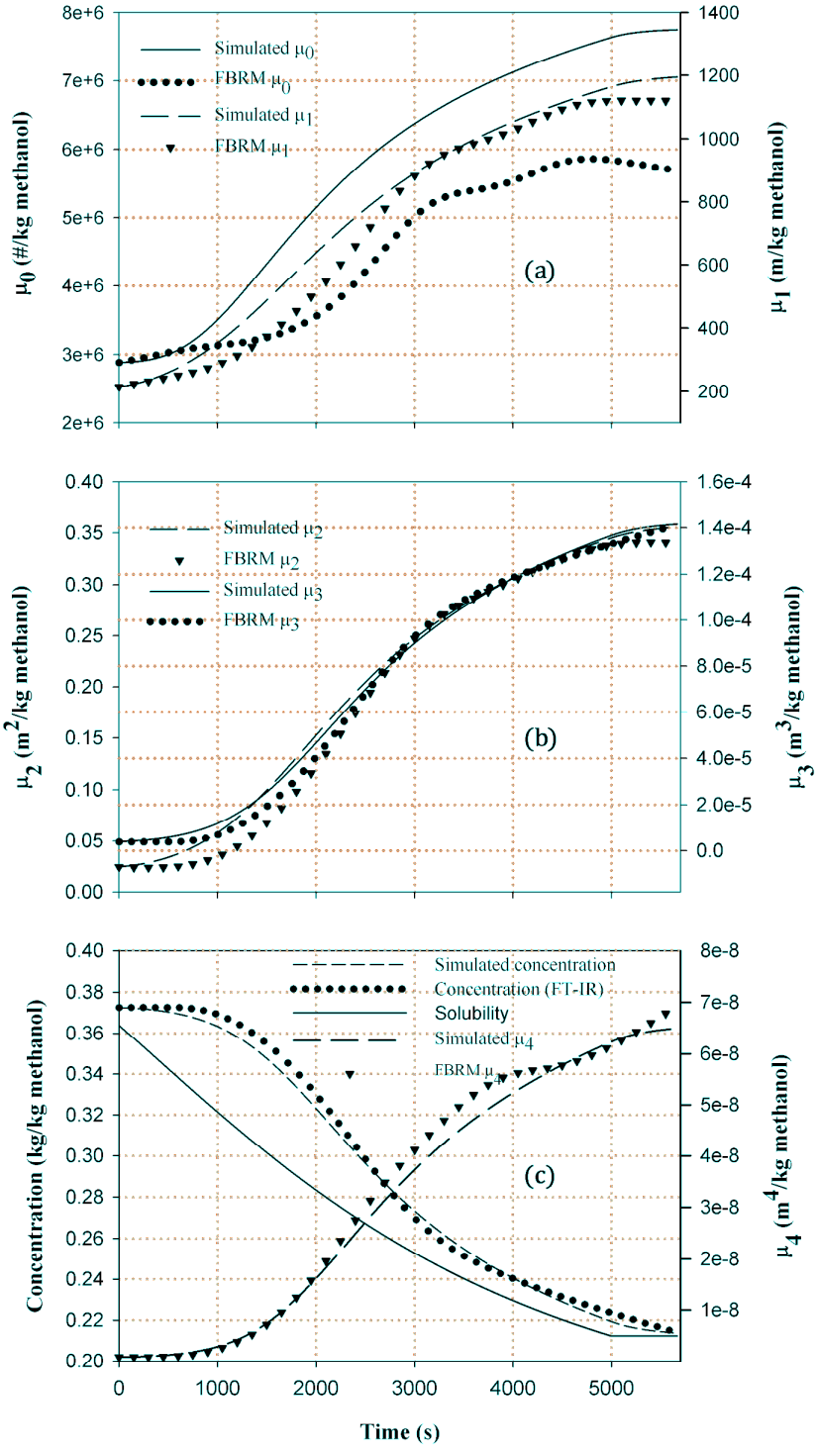


**Figure 3:** Results of Run 3 at a constant addition rate of 3g/min. Overlay plots of experimental FBRM CLD moments calculated using eq 16 and solute concentration against corresponding simulated data. (a) zeroth and first order FBRM moments (b) second and third

order FBRM moments (c) fourth order FBRM moment, experimental solute concentration with corresponding simulated data.

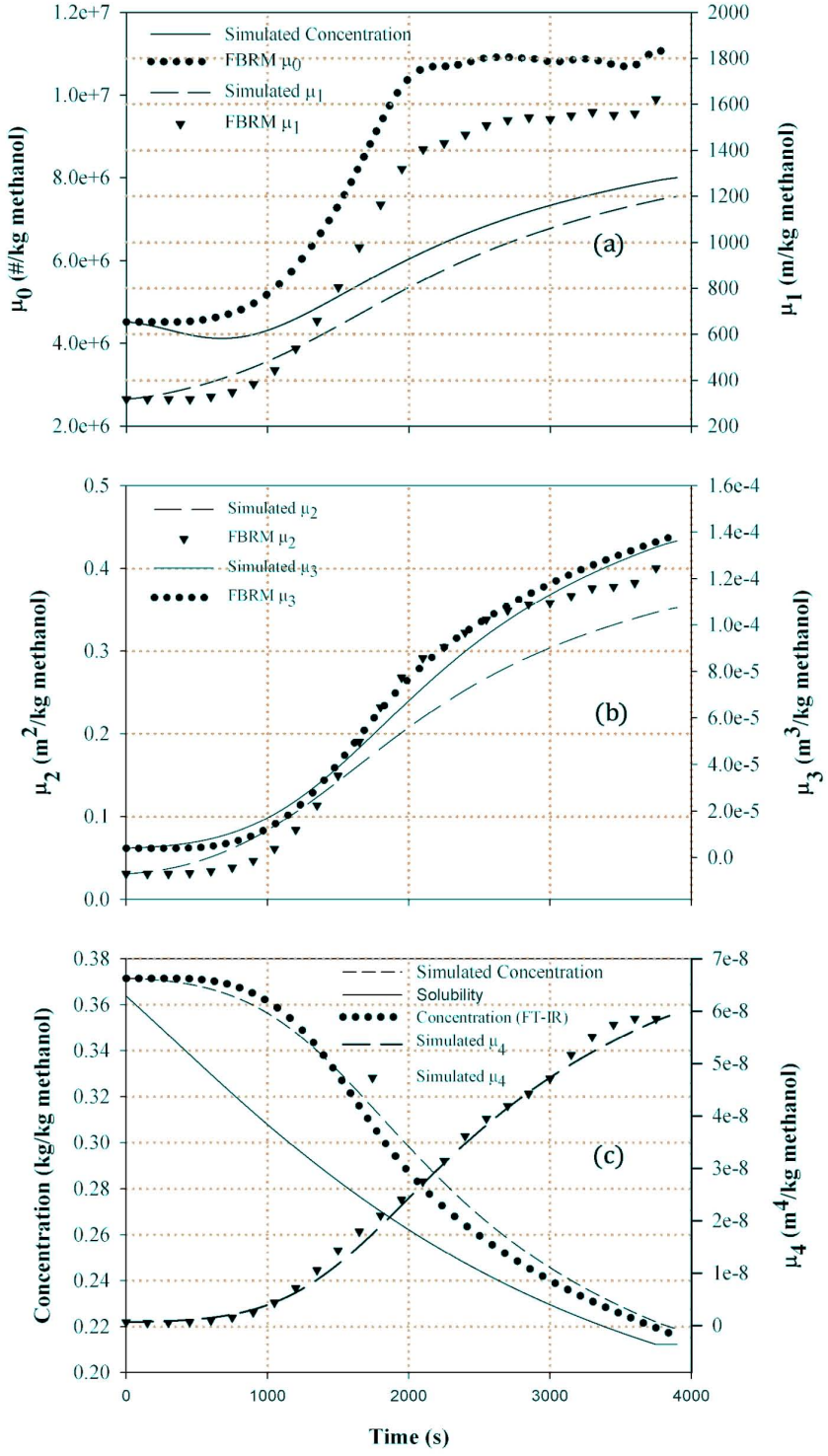

**Figure 4:** Results of Run 4 at a constant addition rate of 4g/min. Overlay plots of experimental FBRM CLD moments calculated using eq 16 and solute concentration against corresponding simulated data. (a) zeroth and first order FBRM moments (b) second and third order FBRM moments (c) fourth order FBRM moment, experimental solute concentration with corresponding simulated data.

The experimental product CSDs for all experiments used in the parameter estimation procedure are also shown as an additional validation of the models predictive capability. Since the simulated CSDs are reconstructed from square weighted CLDs one would expect some discrepancies. Several authors report that square weighted CLDs are comparable to that measured by laser diffraction[15, 16]. However this work shows that there is still some under sizing of CSDs measured by laser diffraction. These discrepancies cannot be attributed to the model as the model regresses FBRM moments and will only reproduce CSDs corresponding to the FBRM measurements. Taking into account these factors the FBRM reproduces the laser diffraction CSDs with reasonable accuracy considering it only measures a chord length and not the total particle diameter. Utilising the gradient of the square weighted CLDs initialised with the seed distribution measured by laser diffraction coupled with concentration data all contribute to achieving this accuracy. All experiments show good agreement with run 3 reproducing the CSD with significant accuracy as can be seen from figure 5.

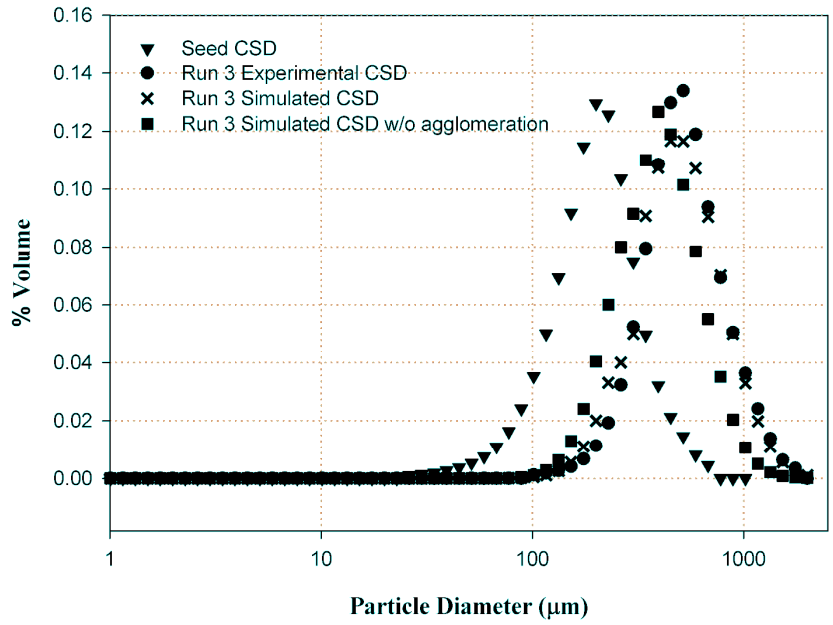

**Figure 5:** Experimental CSD measured by laser diffraction versus the corresponding simulated CSD for Run 3.

Figure 5 also shows the importance of considering agglomeration in your model. The square data points represent a CSD simulated using a model which neglects agglomeration. The biggest and most important discrepancy can be seen for the biggest particles. When compared to simulations without agglomeration the PSD is broader and shifted toward larger particle sizes due to agglomeration. These results are consistent with those of Lindenberg et al also reported this when modelling the L-Glutamic acid system[31]. This demonstrates the importance of considering agglomeration in your model if it presents itself.

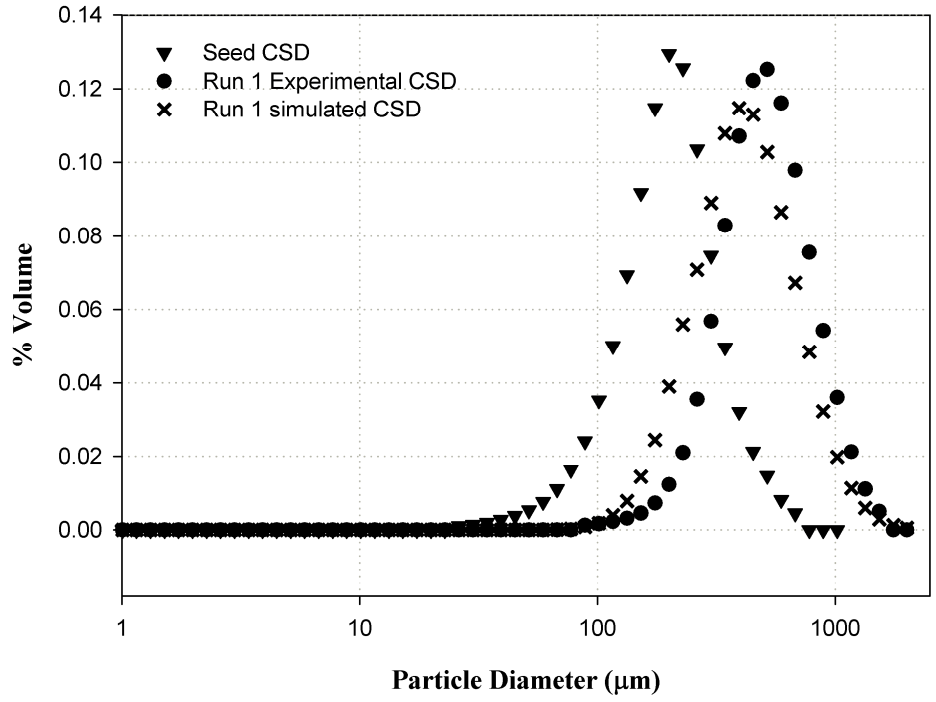


**Figure 6:** Experimental CSD measured by laser diffraction versus the corresponding simulated CSD for Run 1.

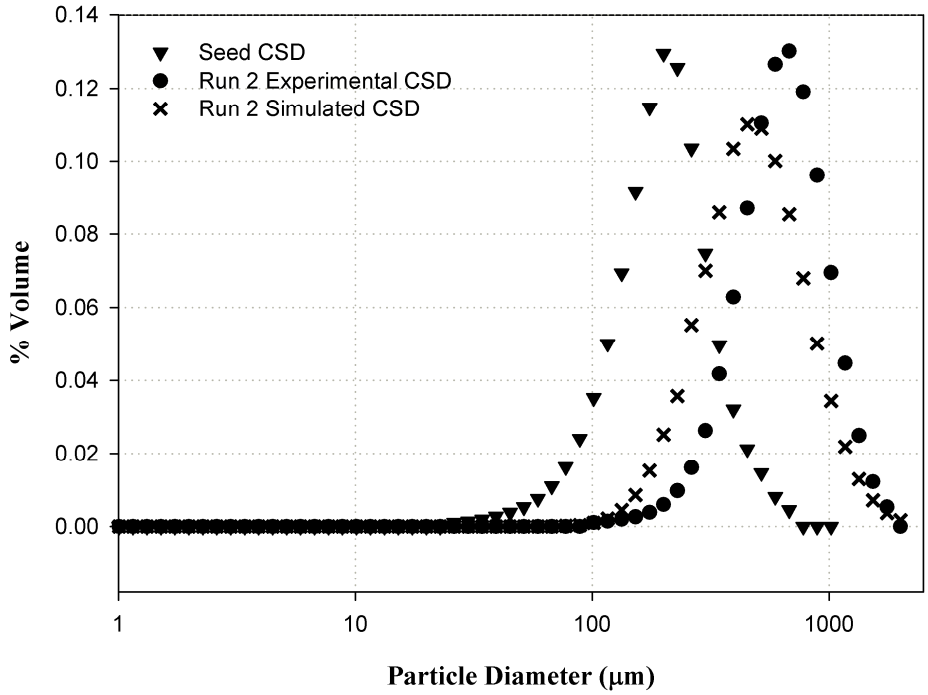


**Figure 7:** Experimental CSD measured by laser diffraction versus the corresponding simulated CSD for Run 2.

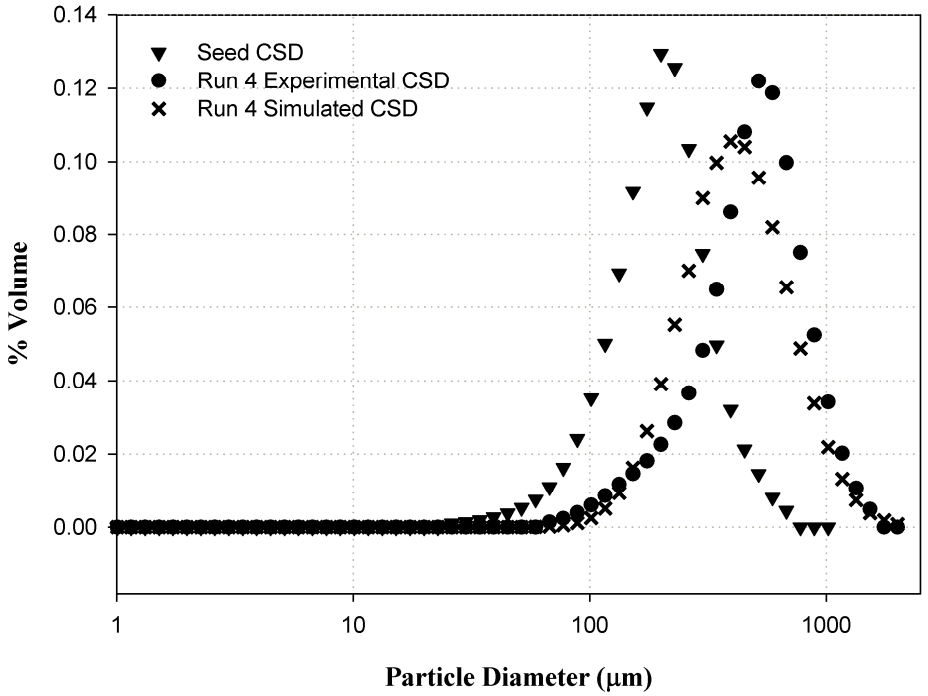


**Figure 8:** Experimental CSD measured by laser diffraction versus the corresponding simulated CSD for Run 4.

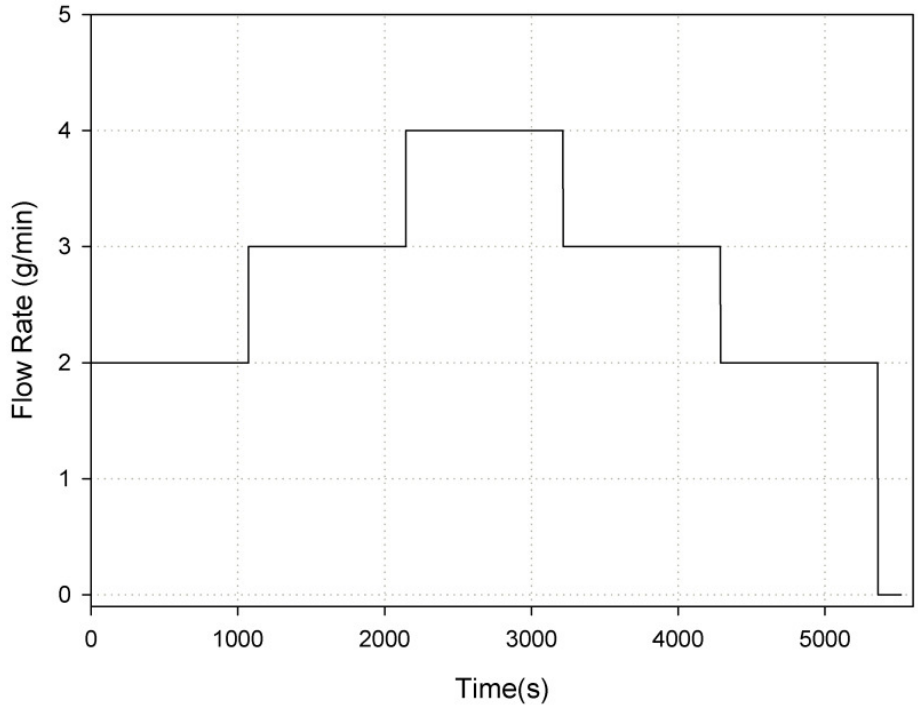


**Figure 9:** Addition rate profile for validation Run 5.

### 4.2 Model validation

#### 4.2.1 Experimental model validation under a new antisolvent addition rate profile

In a further exercise, the testing of the antisolvent crystallization model with the global estimated parameters was undertaken. A new variable antisolvent addition rate was defined arbitrarily and implemented. This addition rate profile is shown in figure 9. Figure 10 shows the predictive ability of the model in predicting moments calculated from FBRM CLDs and solute concentration values calculated from ATR-FTIR calibration procedure.
Overall, this is a satisfactory validation outcome considering the extensive variation of the new antisolvent feed profile. The model also successfully predicts a drop in particle number possibly due to agglomeration. This successfully demonstrates the efficacy of the model in predicting all phenomena occurring during the process.

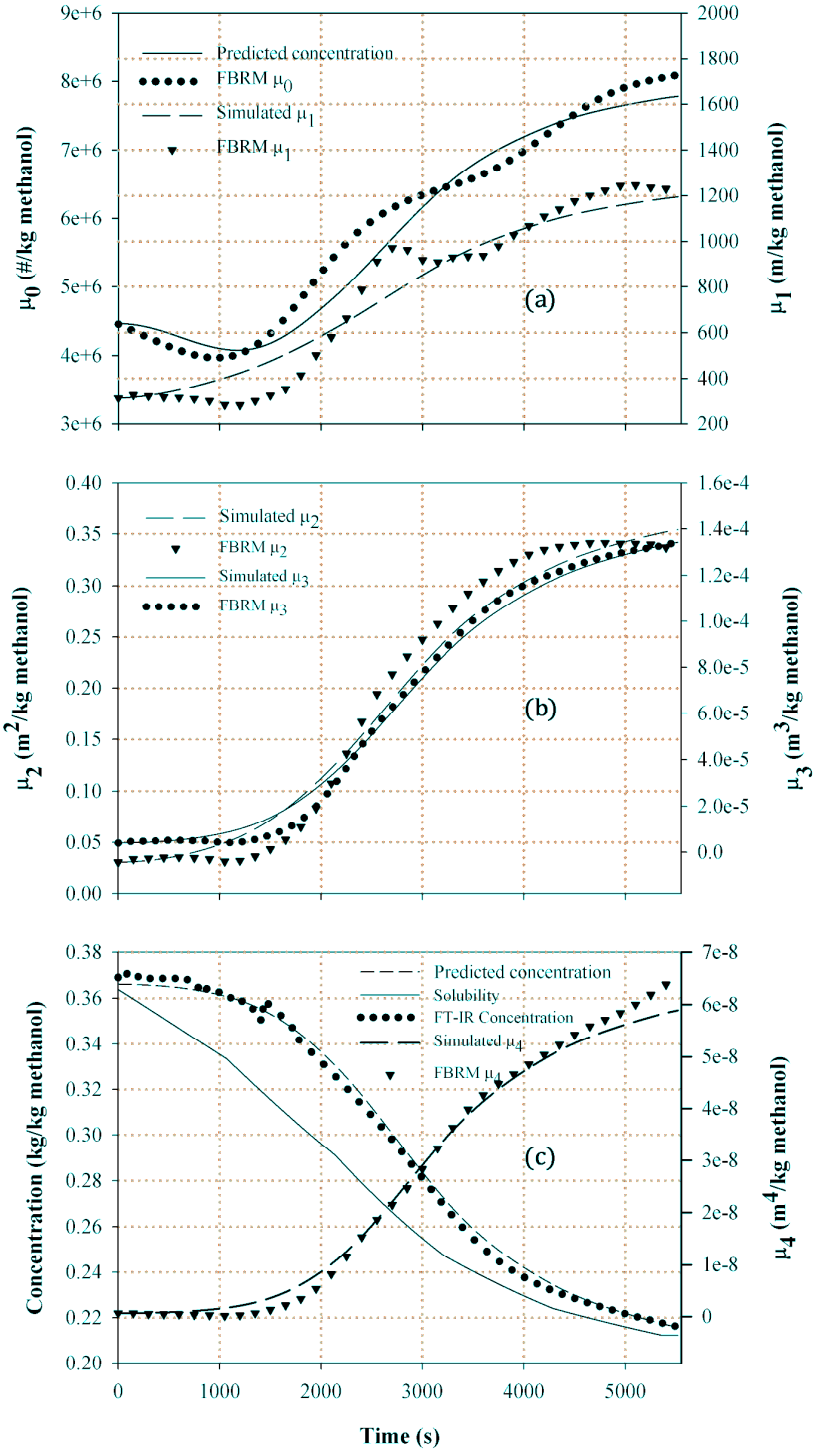


**Figure 10:** Results of validation Run 5 at a variable anti-solvent addition. Overlay plots of experimental FBRM CLD moments calculated using eq 16 and solute concentration against corresponding simulated data. (a) zeroth and first order FBRM moments (b) second and third order FBRM moments (c) fourth order FBRM moment, experimental solute concentration with corresponding simulated data.

### 4.3 Repeatability

In order to investigate the repeatability of the experimental technique, all experiments have been repeated. The lower order moments and experimental solute concentration corresponding to run 3 and run 3 repeat, described in section 4.1 are shown in figure 11. All plots show a high level of repeatability with the exception of the zeroth moment which for reasons already discussed in section 4.1 is the most error prone data set.

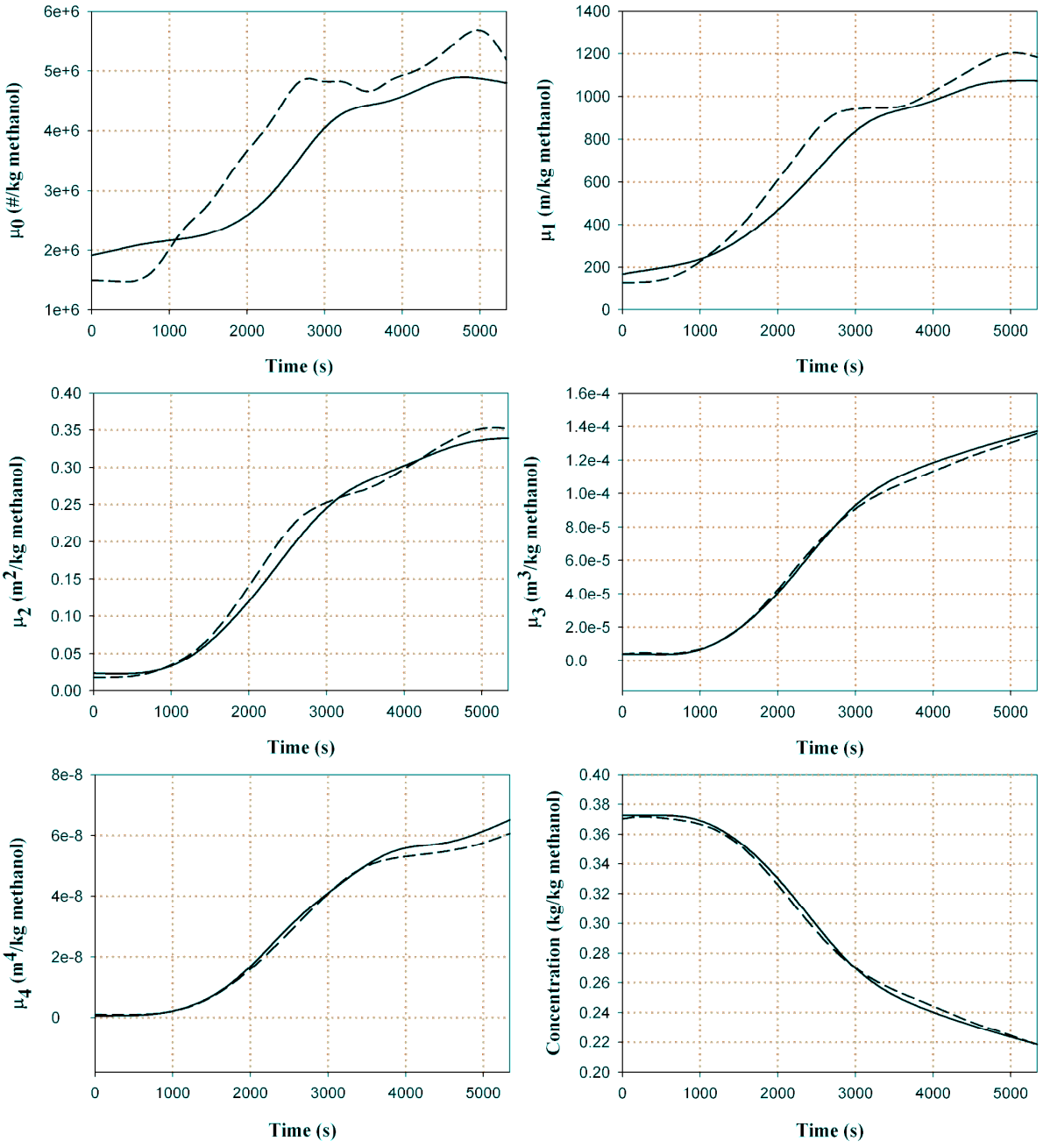

**Figure 11**: Repeatability of run 3 (solid lines run 3. Dashed: run3 repeat) lower order moments and solute concentration

## 5. Process Optimisation.

### 5.1 Results and discussion.

Once the kinetic parameters were estimated to sufficiently high accuracy and the model verified in the additional batch experiment, the model was used to compute an anti-solvent addition profile and seed load that maximises the volume averaged particle diameter, minimizes the coefficient of variation, minimizes the total crystal number ($\mu_0$) and minimizes the total operation time. Addition rate profiles were optimized for each of the optimization objectives for an addition rate profile consisting of 10 linear segments. Increasing the quantity of segments only produced minor improvements. A maximum addition rate of 10g/min to a minimum addition rate of 0.5g/min was employed in the optimisation. Due to the conflicting nature of various optimal targets in batch crystallisation, a multi-objective problem needs to be formulated. In this work a flexible free final time formulation was evaluated and discussed. Several optimisation targets such as large crystal size, narrow CSD, and a reduced operating time are tested with the anti-solvent addition rate profile and the seed mass as decision variables. Several objective functions were considered, and the resulting CSD distributions were compared. In all cases the crystal yield is constrained to be 99.9% of the saturation concentration corresponding to 250g of anti-solvent. Constraints reported in Table 1 were used in all of the objective functions. The solutions of the optimal antisolvent profiles were obtained by applying constrained nonlinear multi-objective optimization algorithms to the crystallization model. The MATLAB optimization function *fminsearchbnd* discussed in section 3.2 was used for solving the optimization problem. This involves minimising a scalar value which is a summation of all optimisation functions discussed above, similar to the parameter estimation procedure described in section 3.2. All objectives in the cost function were equally weighted. The solutions of the optimal antisolvent profiles were obtained by applying constrained nonlinear multi-objective optimization to the crystallization model. Three optimisation problems with alternative trajectories will be discussed and compared. All objectives start with run 2 as an initial estimate. This experiment is also used as a base case to compare the results from the optimisation test cases. This experiment was chosen as a base case as consultations with industry has shown that addition rates in industrial anti-solvent crystallisations are typically low at 1-2g/min.

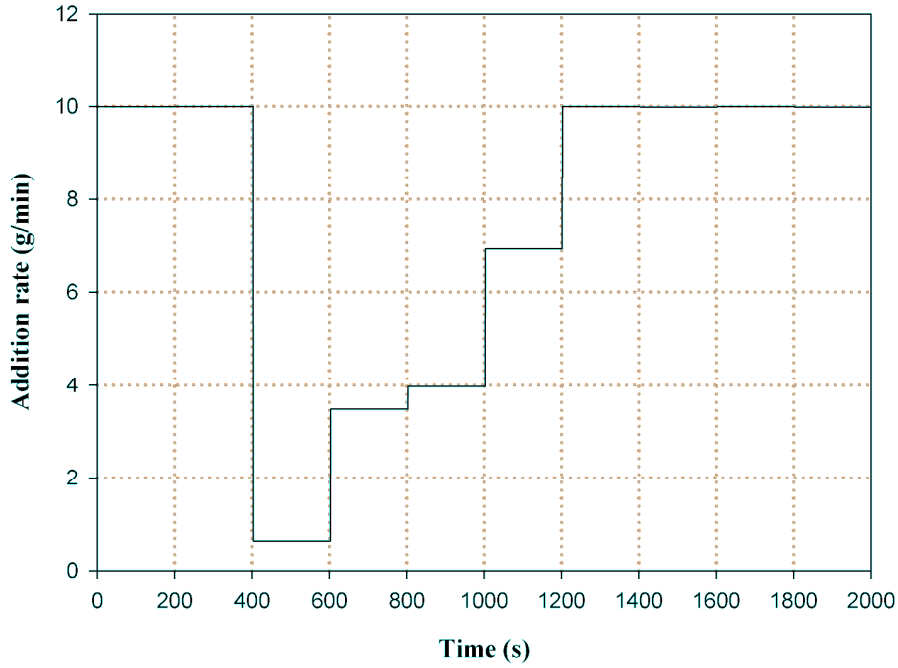


**Figure 12:** Optimal Addition rate profile produced by the conditions laid out in Objective 2

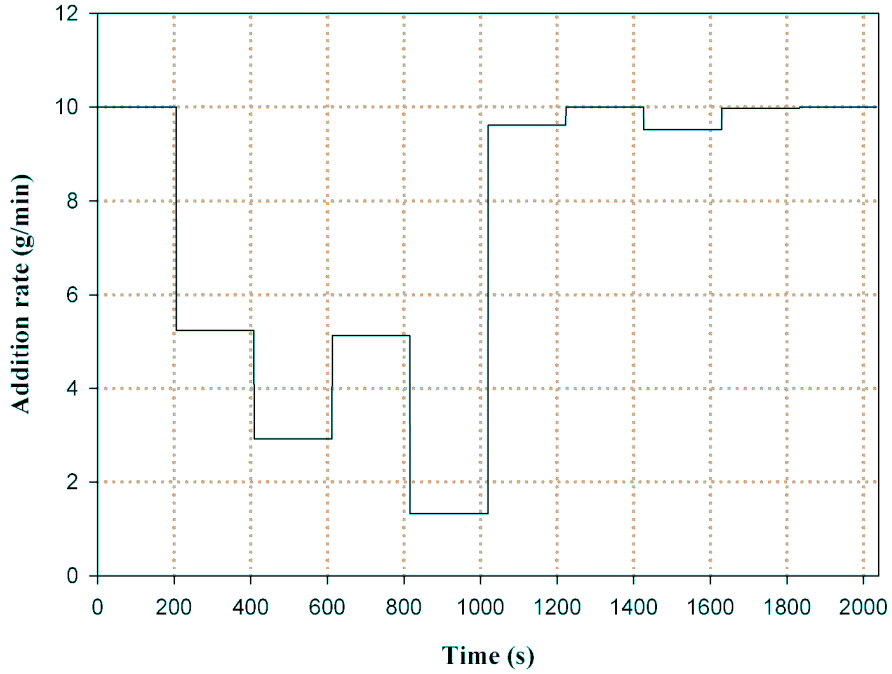


**Figure 13:** Optimal Addition rate profile produced by the conditions laid out in Objective 3

**Objective 1.**

Objective 1 consists of maximizing the mean crystal size (*J11*) and minimizing the coefficient of variation (COV) subject to constraints $g_1$ to $g_4$ with the addition rate and seed mass as decision variables. The minimization of this objective resulted in a 10% increase in batch time, a 7% increase in the COV and only achieved a 1.5% increase in mean crystal size. Based on the simulated results it was decided not to proceed with an experiment analysing the optimised conditions. The objective is shown here to demonstrate the necessity to include batch time as a trajectory in the problem.

$$\begin{cases} \mathbf{max}_{M(t),M_{seed}} J11 = \frac{\mu_4}{\mu_3} \\ \mathbf{min}_{M(t),M_{seed}} J12 = Cov \\ \quad \boldsymbol{subject\ to}\ g_1(t) = C_s > C^* \\ \quad g_2 = mass_{seed}^{Min} \leq mass_{seed} \leq mass_{seed}^{Max} \\ \quad g_3 = \mu_3(t_f) \geq \mu_3(t_f) | Linear\ profile \\ \quad g_4(t) = R_{min}(t) \leq R(t) \leq R_{max}(t) \end{cases} \tag{24}$$

The bound constraints for objective 1 were chosen on the basis of the knowledge gained from the open-loop experiments. The constraint $g_3$ ensures that the yield remains unchanged with every optimal solution found. The values of the yield are always at the saturation concentration corresponding to the amount of mass charged into the crystalliser. This is designed so that the optimiser can find solutions to current processes without impacting on the yield. Since yield is thermodynamic property of the system and can only be increased by a larger addition of solvent and hence reducing the solubility it is not considered as a trajectory.

**Objective 2.**

The objective for the second case was a vector consisting of three single objective functions. In objective 2, final batch time ($J_{22}$) is added to the problem as an additional trajectory. This formulation is aimed at simultaneously improving the CSD product quality and the productivity of the operation and can be stated as:

$$\begin{cases} \mathbf{max}_{M(t),M_{seed}} J21 = \frac{\mu_4}{\mu_3} \\ \mathbf{min}_{M(t),M_{seed}} J22 = t_f \\ \mathbf{min}_{M(t),M_{seed}} J23 = Cov \\ \quad \boldsymbol{subject\ to}\ g_1(t), g_2, g_3, g_4(t) \end{cases} \tag{23}$$

**Objective 3.**

The objective for the third case was a vector consisting of four single objective functions. In objective 3 we seek addition rate profiles and mass of seeds that simultaneously improve the mean size of the product CSD, COV, and batch times.

$$\begin{cases} \mathbf{max}_{M(t),M_{seed}} J31 = \frac{\mu_4}{\mu_3} \\ \mathbf{min}_{M(t),M_{seed}} J32 = t_f \\ \mathbf{min}_{M(t),M_{seed}} J33 = B \\ \mathbf{min}_{M(t),M_{seed}} J34 = Cov \\ \quad \boldsymbol{subject\ to}\ g_1(t), g_2, g_3, g_4(t) \end{cases} \tag{25}$$

Table 3 compares the optimised solutions to that achieved by a linear addition rate for all objective problems. In objective 1, the volume weighted mean crystal size of the crystals can only be increased at the expense of longer batch time and increased COV. This demonstrates the necessity to include process time in the objective function. Thus a product CSD with a large crystal mean size and a small COV in a minimum time of operation is naturally a desired process objective.

**Table 3**: Comparison between end of batch Properties for Different Experiments.

| Strategy | $M_{seed}$ (g)(seed load) | Mean (d4/3) (μm) | COV | $\mu_0$ | Time (min) (% reduction) |
|---|---|---|---|---|---|
| Linear | 0.79 (3%) | 553.71 | 0.4196 | 3.01 x$10^6$ | 125 min |
| Objective 2 | 1.07 (3.9%) | 532.06 | 0.4192 | 1.62 x$10^6$ | 33.3 min (73.3%) |
| Objective 3 | 2.5 (9.16%) | 490.1 | 0.4795 | 2.82 x$10^6$ | 33.9 min (72.8%) |

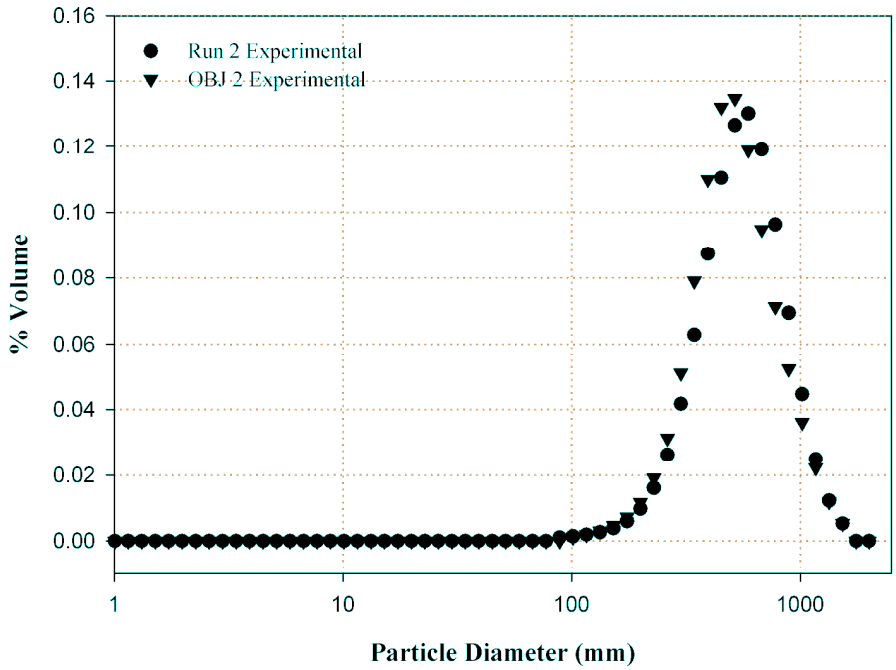


**Figure 14:** Experimental CSDs for objective 2 versus Run 2. CSDs measured by laser diffraction for the base case (run 2: 2g/min) and the corresponding optimised CSD produced by the conditions laid out in Objective 2

Table 3 shows the results and conditions of the optimisation runs namely objective 1 to 3. All results tabulated have been calculated from experimental final product distributions measured by laser diffraction. As can be seen from table 3 objectives 2 and 3 resulted in a significant drop in batch time. Batch time here is considered to be the time taken to add all of the anti-solvent mass which is the same as the base case run 2. An additional length of time is then given by the constraint $g_3$ to push the yield to within 99.9% of the saturation concentration thereby improving the yield in some cases. As can be seen from figure 16 A and B and as reported in table 3, the antisolvent addition stops at 33.3 minutes and the time taken for the solute concentration to reach 99.9 % of the solubility is 13.6 minutes for both objective 2 and 3. Objective 2 resulted in a 73.3% drop in addition time however as consequence a 21.65µm drop in mean crystal size was also observed. Figure 14 compares objective 2 (OBJ 2) with a linear profile (RUN 2). This figure demonstrates that the optimised addition rate shown in figure 12 has had a minor impact on the characteristics of the original CSD. With a minimal increase in seed mass (0.9%) a reduction in addition time, COV and total crystal number defined as ($\mu_0$) was observed. This is surprising result as crystal number was not included as a target in the optimisation problem (OBJ 2). This is a significant result as the cost of the

process is reduced with a minimal impact on the original CSD. In a pharmaceutical process specifications for a CSD in some instances can be very tight and a significant impact on the product CSD would not be desirable. Objective 2 meets this constraint while simultaneously optimising batch time and to a smaller extent fines and COV. These results clearly show the necessity of a multi objective optimisation as many conflicts exist in crystallisation.

In objective 3 an additional target has been added to reduce the total crystal number ($\mu_0$). This objective produces a similar result to objective 2 with respect to batch time however objective 2 produced a greater reduction in fines. Figure 15 illustrates that the optimised addition rate shown in figure 13 has had a minor impact on the characteristics of the original CSD however in this objective an increased reduction in crystal mean size is observed. The optimal seed mass was at the specified upper bound of 2.5g. Figure 16 shows the optimised concentration profiles relating to both objective problems. One can see the effect of this increase in seed mass in figure 16B. The solute concentration can be seen to track the saturation concentration curve over time as increased seed mass reduces the generation of nuclei and supersaturation. This increased consumption of supersaturation can be explained by the increase in total seed surface area available for crystal growth, from the additional seed. A larger seed mass will result in a larger value for the second moment corresponding to the surface area of particles and hence will result in higher decay of supersaturation. This phenomenon has been outlined in some detail by O'Ciardha et al[36]. An increase in seed mass is generally observed when a reduction in crystal number is added as a target to the objective. However a larger reduction in fines is observed in the objective which does not consider fines. An increased quality of fit is observed for OBJ2 and there exists some discrepancies between the experimental and simulated concentration profiles for objective 3 which may explain this unexpected result. In both cases however the CSD remains largely unaffected with significant reduction in batch times.

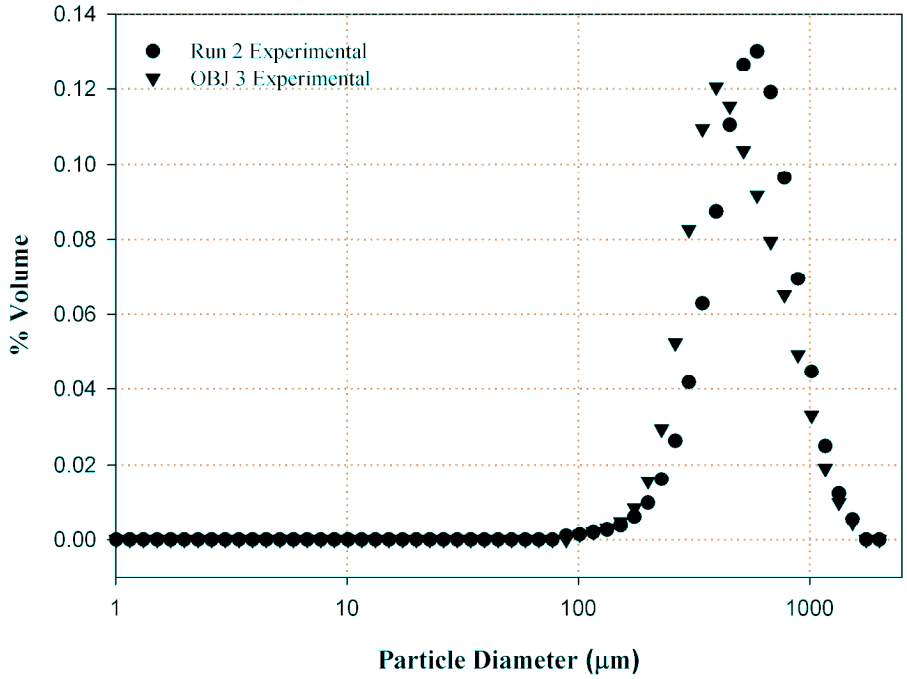


**Figure 15:** Experimental CSDs for objective 3 versus Run 2. CSDs measured by laser diffraction for the base case (run 2: 2g/min) and the corresponding optimised CSD produced by the conditions laid out in Objective 3

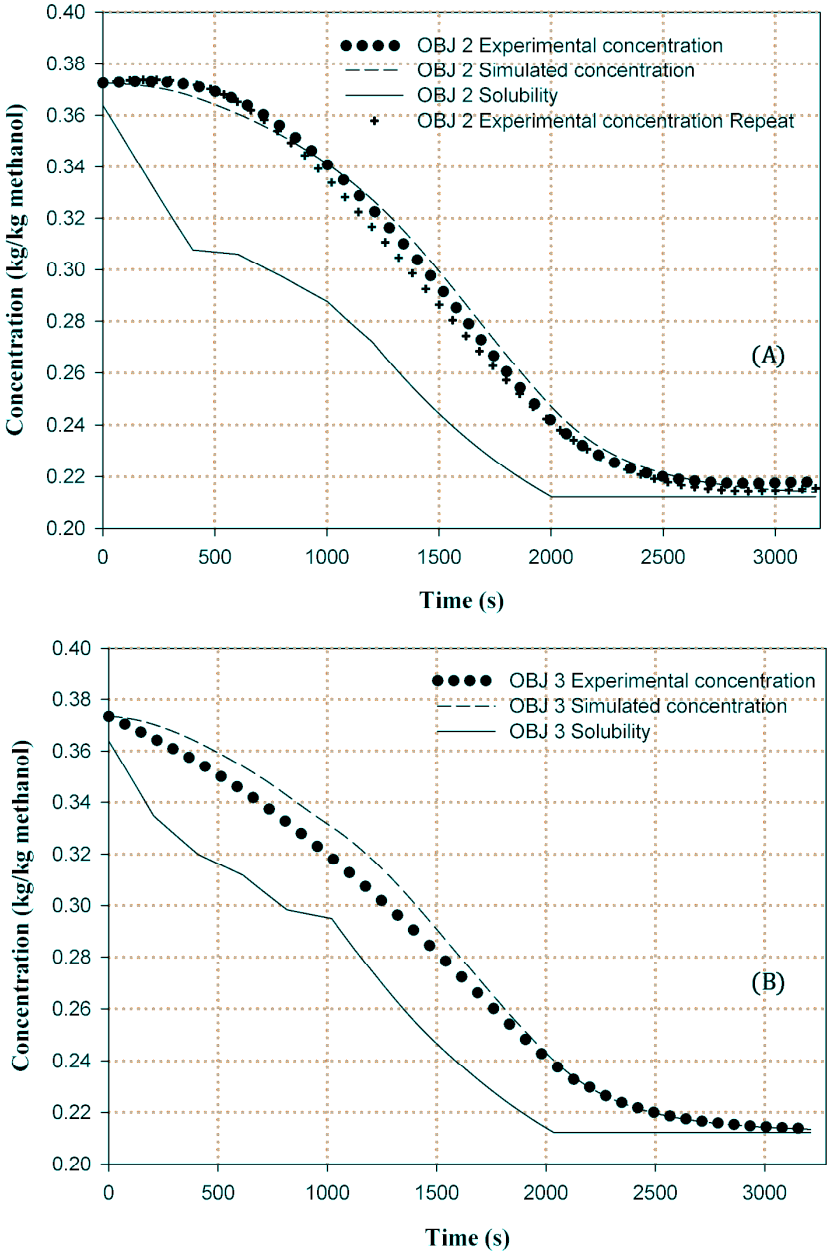


**Figure 16:** Experimental and simulated concentration profiles produced by the conditions laid out in objectives 2 and 3 with their corresponding solubility data.

### 5.2 Trade off analysis

Due to the various tradeoffs in crystallisation an additional step is taken here to give the practitioner more information to make a decision on the optimal operating conditions. Using the case stipulated in objective 3 which considers mean crystal size, batch time, COV and total crystal number the variation of process time coefficient of variation, mean size and

number of nucleated crystals are investigated. In objective 3 the seed mass was a decision variable. In this case the seed mass is locked and an optimal solution is found with just the addition rate. Figure 17 shows all the optimal solutions of problem 3 with varying seed mass. This allows the user to make a decision with more data at hand. For example, no extra reduction in process time can be achieved at any seed loading greater than 20%. This coincides with the greatest reduction in the coefficient of variation which is a measure of the spread of a CSD and hence the filterability of the product slurry. However this also results in a reduction of 14% in the product mean size. Process desirables such as the coefficient of variation, process time and number of nucleated crystals diminish as we desire to obtain product crystals with larger mean size.

The implementation of a trade-off analysis is dependent upon the availability of decision maker's preferences. The decision maker may assign a specific target value that he/she wishes to achieve for each of the objectives. Since different Pareto optimal solutions have different properties, the inspection of the entire Pareto front helps the decision maker in deciding which specifications of the performance objective can be achieved and how the specifications could be traded off in order to find the most suitable operating condition for the process. The multi objective optimization approach clearly opens a wide range of alternatives to the decision maker to operate the system based on practical and feasible consideration.

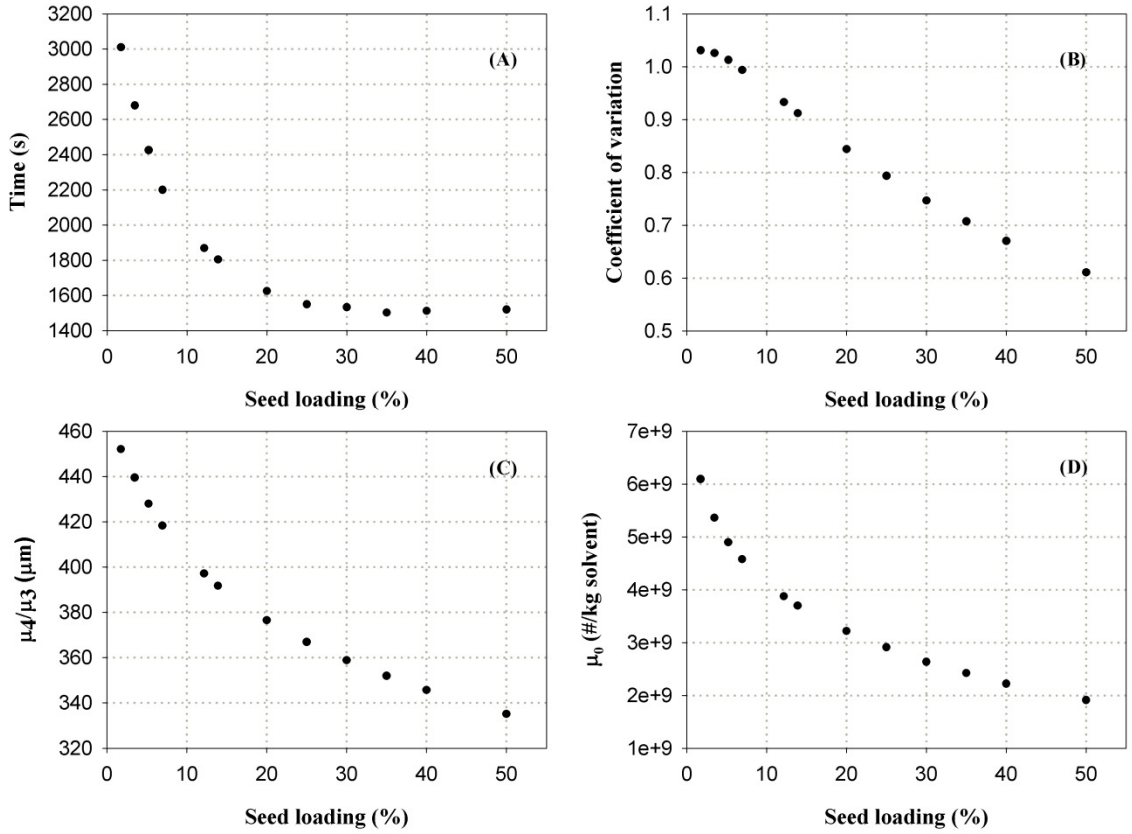


**Figure 17:** (A) Variation of total anti-solvent addition time with seed loading. (B) Variation of the coefficient of variation with seed loading. (C) Variation of average particle size with seed loading. (D) Variation of total crystal number with seed loading.

## 6. Conclusion

In this paper, we have presented a detailed model for an anti-solvent crystallization. The model includes nucleation, growth and agglomeration and is solved with the quadrature method of moments. Optimization based parameter estimated paved the way for the systematic estimation of kinetic parameters. Particle size data is inferred from square weighted FBRM CLDs and solute concentration from ATR-FTIR. FBRM CLDs are coupled with concentration data to conserve yield and this, coupled with the gradient of the FBRM CLDs leads to increased accuracy when calculating moments from the CLDs. The model is shown to fit all experimental data with good agreement and the predicted CSDs are compared to CSDs measured by laser diffraction and are also in good agreement. An additional

validation experiment with a new variable addition rate was performed to test the accuracy of the model and the global parameters are shown to predict the experimental data with good accuracy and low confidence intervals. A multi-objective nonlinear constrained optimisation with a free final time formulation was performed on the validated model to obtain the optimal addition rates to improve selected CSD properties. A significant reduction in process time with minimal reduction in CSD properties was achieved. Additional simulations were also performed to provide more freedom to the user with regards to the effect of seed mass.

## Acknowledgements

This research has been conducted as part of the Solid State Pharmaceuticals Cluster (SSPC) and funded by Science Foundation Ireland (SFI).

## Nomenclature

| *Symbol* | *Description* | *Units* |
|---|---|---|
| $B$ | Particle Birth | $m^{-3}\ s^{-1}$ |
| $C$ | Concentration | kg/kg (methanol) |
| $C^*$ | Equilibrium concentration (solubility) | kg/kg (methanol) |
| $D$ | Particle Death | $m^{-3}\ s^{-1}$ |
| $d_{imp}$ | Impeller diameter | m |
| $G$ | Growth rate | m/s |
| $g$ | Growth order | - |
| $J$ | Nucleation rate | #/kg methanol $s^{-1}$ |
| $J$ | Jacobian | - |
| $k_g$ | Growth Rate Constant | m/s |
| $k_n$ | Nucleation Rate Constant | #/kg methanol $s^{-1}$ |
| $k_v$ | Volume Shape Factor | - |
| $L$ | Particle Diameter | m |
| $m_c$ | Mass of solids | kg |
| $m_s$ | Mass of solvent | kg |
| $m_k$ | $k^{th}$ Moment of Particle Size Distribution | $m^k$ |
| $N_p$ | Power number | - |

| | | |
|---|---|---|
| $N_y$ | Number of measured variables | - |
| $N_{nex}$ | Number of experiments | - |
| $N_d$ | Number of measurement intervals | - |
| $N_{df}$ | Number of degrees of freedom | - |
| $N_i$ | Total number of particles in *i*th channel | - |
| N | Quadrature node | - |
| $n$ | Population Density | $\#/m^4$ |
| $n$ | Nucleation order | - |
| $n_s$ | Stirrer Speed | $\#/s^{-1}$ |
| $n_{sec}$ | Secondary nucleation order | - |
| $P$ | Precision matrix | - |
| $S_R^2$ | Residual variance | - |
| $T$ | Temperature | K |
| $t_{\alpha/2,N\mathrm{df}}$ | $t$ distribution with $N_{\mathrm{df}}$ degrees of freedom | - |
| $t_f$ | Final batch time | s |
| $V$ | Covariance matrix | - |
| $V$ | Solution Volume | $m^3$ |
| $w$ | Parameter estimation weight | - |
| $y_{\mathrm{exp}}$ | Experimental measurement vector | - |
| $y_{\mathrm{sim}}$ | Simulated output vector | - |
| | | |
| $\Delta C$ | Absolute supersaturation | kg/kg (methanol) |
| $\omega$ | Quadrature weighting function | $\#/m^3$ |
| $\varepsilon$ | Energy dissipation rate | $m^2\ s^{-3}$ |
| $\beta$ | Agglomeration kernel | $m^3\ s^{-1}$ |
| $\rho_c$ | Crystal Density | $kg/m^3$ |
| $\theta$ | Parameter set | - |
| o | Initial | - |
| $\lambda$ | Particle Diameter | m |

## References


(1) Doki, N.; Kubota, N.; Yokota, M.; Kimura, S.; Sasaki, S. Production of sodium chloride crystals of uni-modal size distribution by batch dilution crystallization. *Journal of Chemical Engineering of Japan*. **2002** *35,* (11), 1099–1104.
(2) Takiyama, H.; Otsuhata, T.; Matsuoka, M., Morphology of NaCl crystals in drowning-out precipitation operation, *Trans IChemE Part A: Chem Eng Res Des*, **1998,** 76: 809–814.
(3) Ma, D. L.; Chung. S. H.; Braatz, R. D. Worst-Case Performance Analysis of Optimal Batch Control Trajectories. *AIChE J.* **1999**, *45*, 1469.
(4) Ma, D. L.; Tafti, D. K.; Braatz, R. D. Optimal Control and Simulation of Multidimensional Crystallization Processes. *Comput. Chem. Eng.* **2002**, *26*, 1103.
(5) Nagy, Z. K.; Braatz, R. D. Open-Loop and Closed-Loop Robust Optimal Control of Batch Processes Using Distributional and Worst-Case Analysis. *J. Process Control* **2004**, *14*, 411.
(6) Nagy, Z. K.; Braatz, R. D. Robust Nonlinear Model Predictive Control of Batch Processes. *AIChE J.* **2003**, *49*, 1776.
(7) Rawlings, J. B.; Miller, S. M.; Witkowski, W. R. Model Identification and Control of Solution Crystallization Processes: A Review. *Ind. Eng. Chem. Res.* **1993**, *32*, 1275.
(8) Sarkar, D.; Rohani, S.; Jutan, A. Multi-Objective Optimization of Seeded Batch Crystallization Processes. *Chem. Eng. Sci.* **2006**, *61*, 5282.
(9) Togkalidou, T.; Tung, H. H.; Sun, Y.; Andrews, A. T.; Braatz, R. D. *Ind. Eng. Chem. Res.* **2004**, *43*, 6168-6181.
(10) Worlitschek, J.; Mazzotti, M. Model-Based Optimization of Particle Size Distribution in Batch-Cooling Crystallization of Paracetamol *Cryst. Growth Des.* **2004**, *4*, 891- 903.
(11) Miller, S. M.; Rawlings, J. B. Model identification and control strategies for batch cooling crystallizers, *AIChE J.* **1994**, *40*, 1312-1327.
(12) Hermanto, M.W.; Chow, P.S.; Tan, R.B.H. Implementation of Focused Beam Reflectance Measurement (FBRM) in Antisolvent Crystallization to Achieve Consistent Product Quality *Crystal Growth & Design*. **2010** *10,* (8), 3668–3674.
(13) Barrett, P.; Glennon, B. In-line FBRM Monitoring of Particle Size in Dilute Agitated Suspensions *Part. Part. Syst. Charact*. **1999,** *16,* 207-211.
(14) Leyssens, T.; Baudry, C.; Hernandez, M.L.E. Optimization of a Crystallization by Online FBRM Analysis of Needle-Shaped Crystals, *Org. Process Res. Dev*. **2011**, *15*, 413–426.
(15) Heath, A.R.; Fawell, P.D.; Bahri, P.A.; Swift. J.D. Estimating Average Particle Size by Focused Beam Reflectance Measurement (FBRM), *Part. Part. Syst. Charact*. **2002**, *19* 84 - 95.
(16) Yu, Z.Q.; Chow, P.S.; Tan, R.B.H. Interpretation of Focused Beam Reflectance Measurement (FBRM) Data via Simulated Crystallization *Organic Process Research & Development,* 2008**,** *12,* 646–654.
(17) Kail, N.; Marquardt, W.; Briesen, H. Process Analysis by Means of Focused Beam Reflectance Measurements., *Ind. Eng. Chem. Res.* **2009,** *48,* 2936–2946
(18) Fischer, C.; Peglow, M.; Tsotsas, E. Restoration of particle size distributions from fiber-optical in-line measurements in fluidized bed processes. *Chemical Engineering Science*, **2011**, *66,* 2842–2852.
(19) Pons, M.N.; Milferstedt, K.; Morgenroth. E. Modeling of chord length distributions *Chemical Engineering Science* **2006,** *61*, 3962 – 3973.
(20) Worlitscheck, R.; Mazzotti, M. Modelling and experimental analysis of CSD measurements through FBRM. *Part. Part. Syst. Charact*. **2000**, *17,* 167-179.

(21) Wynn, E.J.W. Relationship between particle-size and chord-length distributions in focused beam reflectance measurement: stability of direct inversion and weighting Powder Technology. **2003**, *133,*125– 133.
(22) Li, M.; Wilkinson, D.; Patchigolla, K. Determination of non-spherical particle size distribution from chord length measurements. Part 2: Experimental validation *Chemical Engineering Science* **2005,** *60*, 3251 – 3265.
(23) Togkalidou, T.; Tung, H.H.; Sun, Y.; Andrews, A.T.; Braatz, R.D. Parameter Estimation and Optimization of a Loosely Bound Aggregating Pharmaceutical Crystallization Using in Situ Infrared and Laser Backscattering Measurements, *Ind. Eng. Chem. Res.* **2004,** *43,* 6168-6181.
(24) Trifkovic, M.; Sheikhzadeh, M.; Rohani, S. Kinetics Estimation and Single and Multi-Objective Optimization of a Seeded, Anti-Solvent, Isothermal Batch Crystallizer. *Ind. Eng. Chem. Res.*, **2008**, *47* (5), 1586-1595.
(25) Zoltan K. Nagy, A. Population balance model approach for crystallization product engineering via distribution shaping control**,** *Computer Aided Chemical Engineering* Volume, **2008***, 25*, 139–144
(26) Seyssiecq, L.; Veesler, S.; Mangin, D.; Klein, J. P.; Boistelle, R. Modelling gibbsite agglomeration in a constant supersaturation crystallizer, *Chemical Engineering Science,* **2000,** *55,* 5565-5578.
(27) Livk, I.; Gregorkaa, M.; Model Identification of batch crystallisation processes (Estimate of kinetic parameters of sodium-perborate precipitation), *Computers chem Engng supplement,* **1995***, 19 1*, *11–14 June*, *241-246.*
(28) O'Ciardha, C. T.; Mitchell, N. A.; Hutton, K. W.; Frawley, P. J. Determination of the Crystal Growth Rate of Paracetamol As a function of solvent composition, *Ind. Eng. Chem. Res.*, **2012**, *51* (12), 4731–4740.
(29) Rawlings, J.B.; Miller, S.M.; Witkowski, W.R. Model identification and control of solution crystallization processes: a review; *Ind. Eng. Chem. Res.*, **1993**, 32 (7), 1275-1296
(30) Chapple, D.; Kresta, S.M.; Wall, A.; Afacan, A.; The Effect of impeller and tank geometry on power number for a pitched blade turbine, *Trans. IChemE*, **2002**, *80* (A) 364-372.
(31) Lindenberg, C.; Schöll, J.; Vicum, L.; Mazzotti, M.; Brozio. J. L-Glutamic Acid Precipitation: Agglomeration Effects, *Cryst. Growth Des.* **2008**, *8* (1), 224–237.
(32) Brittain, H.G.; (ED), Polymorphism in Pharmaceutical Solids, Marcel Dekker Inc., New York, 1999.
(33) Hutton, K.; Mitchell, N.; Frawley, P.J. *Powder Technology,* **2012,** *222*, 8–14.
(34) Marchisio, D.L., Vigil, R.D. & Fox, R.O., 2003. Quadrature Method of Moments for Aggregation-Breakage Processes. *Journal of Colloid and Interface Science*, 258, p. 322-334.
(35) Hutton, K. Mathematical modelling of gibbsite precipitation, Ph.D. Thesis, University of Limerick, Ireland, (2009).
(36) Ó'Ciardhá, C.T.; Mitchell, N.A.; Frawley, P.J.; Estimation of the nucleation kinetics for the anti-solvent crystallisation of paracetamol in methanol/water solutions, *J. Cryst Growth.* **2011**, *328,* 50–57.
(37) Beck, J. V.; Arnold, K. J. *Parameter Estimation in Engineering and Science*; Wiley: New York, 1977.

**For table of contents use only**

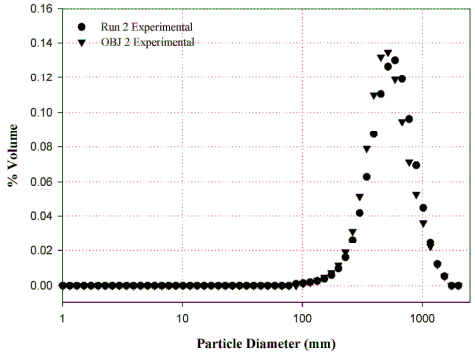


**Figure 13:** Experimental CSDs for objective 2 versus Run 2.

**Synopsis:**

A population balance incorporating nucleation, growth and agglomeration was coupled with a parameter estimation procedure. All parameters concerned were regressed from moments calculated using the measured square weighted chord length distribution (CLD) generated by the FBRM. Based on the kinetic parameters estimated using the above method, the solution to the optimal anti-solvent addition rate profiles was obtained by applying nonlinear constrained multi-objective free final time formulation optimization on the validated model. A 73.3% reduction in batch time was achieved with little impact on the CSD. Analyses of the various conflictions are presented with the aid of a pareto optimal plot to provide the practitioner with increased flexibility.